HHS Public Access

Author manuscript

Exp Neurol. Author manuscript; available in PMC 2024 March 23.

Published in final edited form as:

Exp Neurol. 2023 August ; 366: 114445. doi:10.1016/j.expneurol.2023.114445.

PRMT7 can prevent neurovascular uncoupling, blood-brain barrier permeability, and mitochondrial dysfunction in repetitive and mild traumatic brain injury

Christina H. Acosta[a], **Garrett A. Clemons**[a], **Cristiane T. Citadin**[a], **William C. Carr**[b], **Mariana Sayuri Berto Udo**[b], **Vesna Tesic**[b], **Henry W. Sanicola**[b,c], **Anne H. Freelin**[c], **Jamie B. Toms**[c], **J. Dedrick Jordan**[b], **Bharat Guthikonda**[c], **Krista M. Rodgers**[a], **Celeste Yin-Chieh Wu**[b], **Reggie Hui-Chao Lee**[b], **Hung Wen Lin**[a,b,*]

[a]Department of Cellular Biology & Anatomy, Louisiana State University Health Sciences Center, Shreveport, LA, United States of America

[b]Department of Neurology, Louisiana State University Health Sciences Center, Shreveport, LA, United States of America

[c]Department of Neurosurgery, Louisiana State University Health Sciences Center, Shreveport, LA, United States of America

Abstract

Mild traumatic brain injury (TBI) comprises the largest percentage of TBI-related injuries, with pathophysiological and functional deficits that persist in a subset of TBI patients. In our three-hit paradigm of repetitive and mild traumatic brain injury (rmTBI), we observed neurovascular uncoupling via decreased red blood cell velocity, microvessel diameter, and leukocyte rolling velocity 3 days post-rmTBI via intra-vital two-photon laser scanning microscopy. Furthermore, our data suggest increased blood-brain barrier (BBB) permeability (leakage), with corresponding decrease in junctional protein expression post-rmTBI. Mitochondrial oxygen consumption rates (measured via Seahorse XFe24) were also altered 3 days post-rmTBI, along with disrupted mitochondrial dynamics of fission and fusion. Overall, these pathophysiological findings correlated with decreased protein arginine methyltransferase 7 (PRMT7) protein levels and activity post-rmTBI. Here, we increased PRMT7 levels *in vivo* to assess the role of the neurovasculature and mitochondria post-rmTBI. *In vivo* overexpression of PRMT7 using

*Corresponding author at: Department of Neurology, LSU Health Sciences Center Shreveport, 1501 Kings Hwy, Shreveport, LA 71103-3932, United States of America. hungwen.lin@lsuhs.edu (H.W. Lin).

Author contributions

Christina H. Acosta provided data curation and formal analysis, conceptualization, and writing of the original draft and editing of the manuscript. Garrett A. Clemons assisted in the data curation and formal analysis of the two-photon microscopy experiments and provided scientific input by investigation and methodology. Cristiane T. Citadin assisted in data curation and formal analysis of real-time qPCR and mitochondrial bioenergetic experiments. Mariana Sayuri Berto-Udo, Vesna Tesic, and William C. Carr assisted in data curation and formal analysis of the manuscript. Henry W. Sanicola, Anne H. Freelin, Jamie B. Toms, Joseph D. Jordan, Bharat Guthikonda, Celeste Yin-Chieh Wu, Reggie Hui-Chao Lee, contributed to the conceptualization of the manuscript. Krista M. Rodgers provided methodology and supervision of the whisker stimulation studies. Hung Wen Lin provided conceptualization, funding acquisition, investigation, methdology, project administration, resources, supervision, validation, and writing of the original draft and provided final editing of the manuscript.

Declaration of Competing Interest

The authors declare that they have no known competing financial interests or personal relationships that could have appeared to influence the work reported in this paper.

a neuronal specific AAV vector led to restoration of neurovascular coupling, prevented BBB leakage, and promoted mitochondrial respiration, altogether to suggest a protective and functional role of PRMT7 in rmTBI.

Keywords

Protein arginine methyltransferase; Cerebral blood flow; Leukocyte rolling; Blood-brain barrier; Mitochondrial dysfunction; Bioenergetics; Gliosis; Traumatic brain injury

1. Introduction

Traumatic brain injury (TBI) can be caused by a penetrating force, hit to the head, or rotating injury from high impact sports, falls, and/or automobile accidents (C. Xu et al., 2022), (Cheng et al., 2019), (Namjoshi et al., 2014). TBI-related injuries manifest as a myriad of physiological, behavioral, and neuropsychiatric symptoms that can persist months to years (Das et al., 2022; Howe et al., 2022). Mild TBI, contributes to the largest proportion of TBI injuries and can have detrimental neurodegenerative outcomes as repetitive injuries accumulate over time (Moro et al., 2022). In addition, TBI is a heterogeneous disorder that has a multitude of pathologies (Das et al., 2022), such as: cerebral blood flow (CBF) derangements (Das et al., 2022), (Stephens et al., 2018), (Li et al., 2020), blood-brain barrier (BBB) permeability/leakage (George et al., 2022), (Szarka et al., 2019), (Huang et al., 2023), and mitochondrial dysfunction (Sun et al., 2022) (Demers-Marcil and Coles, 2022), (Du et al., 2022), (S. Zhang et al., 2022), which all serve as areas of possible intervention.

In fact, decreased CBF post-TBI can increase the severity of injury as well as functional deficits (Ware et al., 2020), (Vedung et al., 2022). Disruption of the BBB can occur early after injury; and in some cases, persist years after injury often associated with poor outcomes (Cash and Theus, 2020). BBB leakage can occur even after a single mild TBI hit in humans, as detected via magnetic resonance imaging (George et al., 2022), (Johnson et al., 2013), (Wang and Li, 2016). Furthermore, leukocytes, as well as platelet aggregation (due to possible hemorrhage), have been observed to bind to the endothelium (via adhesion molecules) and migrate to the parenchyma to further contribute to secondary damage post-TBI (Hartl et al., 1997), (Schwarzmaier et al., 2010), (Schwarzmaier et al., 2013). Moreover, the brain is thought to consume ~20% of the body's oxygen consumption for oxidative phosphorylation and subsequent ATP production, therefore, even the slightest disturbance in mitochondrial bioenergetics and/or dynamics can have profound detrimental outcomes on neuronal function (Vagnozzi et al., 2007), (Kim et al., 2017). Repetitive and mild TBI (rmTBI) can cause mitochondrial dysfunction (Vagnozzi et al., 2007), (Balasubramanian et al., 2021) by altering oxygen consumption rates, as well as mitochondrial fission and fusion dynamics, that can affect overall functional outcomes in rmTBI patients (Khacho et al., 2017), (Moore et al., 2020).

Protein arginine methyltransferase 7 (PRMT7) is an emerging therapeutic target in various pre-clinical and clinical disease pathologies, such as in cancer (Oksa et al., 2022), (C. Liu et al., 2022), metastasis (L. Liu et al., 2021), delayed developmental disorders in humans (Poquerusse et al., 2022), (Agolini et al., 2018), and impaired social skills in

murine knockout models (S. Y. Lee et al., 2020), (W. Zhang et al., 2021), (S. Y. Lee et al., 2019), (Ma et al., 2022), (Fiorica and Wheeler, 2019). PRMT7 has been shown to methylate the sodium leak channel, whereas PRMT7 knockout mice led to intrinsically higher neuronal excitability in the hippocampal dentate granule cells v. wild-type, to suggest PRMT7-mediated methylation is necessary to maintain neuronal resting membrane potential (S. Y. Lee et al., 2019). Additionally, the absence or knockdown of PRMT7 caused a decrease in hyperpolarization-activated cyclic nucleotide-gated channels protein levels and increased resting membrane potential of the CA1 region of the hippocampus (S. Y. Lee et al., 2020), further highlighting the importance of PRMT7 in learning/memory function. Furthermore, our recent investigations suggest a role for PRMT7 in our previous rmTBI studies that correlated with pathologies such as neuroinflammation (Acosta et al., 2023). This correlation between PRMT7 deficiency and pathology set the foundation for this study to investigate a functional role of PRMT7 by using AAV gene therapy. Here, we report that the *in vivo* overexpression of PRMT7 prevented neurovascular uncoupling, BBB permeability/leakage, increased leukocyte rolling, and improved mitochondrial function, to further delineate a functional role for PRMT7 in rmTBI.

2. Materials & methods

2.1. Animal preparation

All experimental procedures were approved by the Institutional Animal Care and Use Committee of the Louisiana State University Health Sciences Center Shreveport. C57BL/6J male mice were purchased from Jackson Laboratory at 7 weeks old. Male mice ages 8–12 weeks, weighing approximately 20–32 g. Mice were held in standard LSU health veterinary conditions with a controlled climate and a 12-h light to dark cycle. Upon completion of rmTBI experimentation, mice were placed into an induction chamber at (5% isoflurane and 900 cc of O_2) for sacrifice. Mice were randomly placed into the following experimental groups: SHAM, SHAM + PRMT7-AAV, 3 days post-rmTBI, 3 days post-rmTBI + PRMT7-AAV, 7 days post-rmTBI, and 7 days post-rmTBI + PRMT7-AAV to assess molecular changes *in vivo*.

2.2. Experimental paradigm

The CHIMERA was utilized for the experimental model of rmTBI. Age-matched male mice (8–12 weeks) were anesthetized using 5% isoflurane and 900 cc of O_2 for 2 min followed by placement onto the CHIMERA apparatus. Mice were maintained using a nose cone and a heat lamp was placed over each mouse to prevent hypothermia-induced neuroprotection (Busto et al., 1989; Dietrich and Bramlett, 2010). After equal duration of anesthesia (~ 4–5 min), the mice were either removed immediately (SHAM) or subjected to a TBI hit (0.7 J). SHAM mice were exposed to anesthesia and O_2 only (no hit) or rmTBI, once daily for 3 days. Overexpression of PRMT7-AAV in C57BL/6J mice was achieved via injection of AAV/PHP.eB-hSYN1-GFP.mPRMT7-WPRE 3–4 weeks prior to rmTBI to enable maximum overexpression prior to rmTBI. PRMT7-AAV overexpressed mice were then exposed to anesthesia (SHAM) or rmTBI once daily for 3 days.

2.3. In vivo overexpression of neuronal PRMT7 via adeno-associated virus

The viral vector AAV/PHP.eB-hSYN1-GFP.mPRMT7-WPRE was purchased from Vector BioLabs (lot number: 220207#39; serotype AAV/PHP.eB) and diluted in Lactated Ringer's solution upon injection. Overexpression virus was injected intravenously at 1×10^{11} vectors/genome into each mouse (Couto et al., 2021). Four weeks later, overexpression of PRMT7-AAV was validated via qRT-PCR and ProteinSimple® analyses in mouse hippocampus and cortex tissue samples. In addition, overexpression was validated via histological sections visualized by confocal microcopy of GFP-tagged PRMT7-AAV in mouse brain sections.

2.4. Real-time quantitative reverse transcription polymerase chain reaction (RT-qPCR)

RNA was extracted using the QIAGEN RNeasy Mini Kit (Cat. No. 74104, QIAGEN, Hilden, Germany). RNA samples were assessed using the NanoDrop (Model: NanoDrop One; serial number: AZY1706087; Thermo Fisher Scientific, Waltham, MA). cDNA was synthesized from 500 ng of extracted mRNA with SuperScript™ III Reverse Transcriptase (Cat. No. 18080051, Thermo Fisher Scientific, Waltham, MA). qPCR was performed in a CFX96 Real-Time PCR Detection System using iQ™ SYBR® Green Supermix (Cat. No. 1708886, Bio-Rad, Hercules, CA). The PCR reaction was as follows: 0.4 µl of cDNA, 10 µl of iQ™ SYBR® Green Supermix (Invitrogen, Carlsbad, CA), 200 nM of each primer, and nuclease free water. The cycling conditions for the qPCR amplification were as follows: 95 °C for 3 mins, 95 °C for 10 s, 60 °C for 30 s, for 40 cycles. Target genes were normalized with the house-keeping gene GAPDH (forward 5'-CATCACTGCCACCCAGAAGACTG-3′ and reverse 5'-ATGCCAGTGAGCTTCCCGTTCAG-3′) (Narayan and Kumar, 2012). The mouse primer sequence for PRMT7 gene was obtained from Primer Bank (ID 21703807c1) database and synthesized by MilliporeSigma (MilliporeSigma, Burlington, MA) (forward 5'-TTGCCAGGTCATCCTATGCC-' and reverse 5'-GCCAATGTCAAGAACCAAGGC −3′).

2.5. Capillary-based immunoassay via ProteinSimple®

Capillary electrophoresis immunoassay (Simple Western analyses) was performed using the Wes/Jess™, according to the manufacturer's protocol (ProteinSimple®, Bio-techne, Minneapolis, MN). Proteins were extracted from tissue lysates using T-PER® Tissue Protein Extraction Reagent (Cat. No. 78510, Thermo Fisher Scientific, Waltham, MA) with Halt™ Protease Inhibitor Cocktail (Cat. No. 87785, Thermo Fisher Scientific, Waltham, MA). Tissue lysates were diluted in sample buffer (Protein Simple®) (1 µg/µl) and added to a fluorescent marker with dithiothreitol. Samples were denatured at 95 °C for 5 mins. Capillary cartridges with a target protein size of 12–230 kDa were used for analysis. Antibodies were diluted in the manufacturer provided antibody diluent (Protein Simple, Bio-techne, Minneapolis, MN) as follows: PRMT7 (1:100; D1K6R, Cell Signaling Technology, Danvers, MA), MMA (1:50; 8015S, Cell Signaling), DRP1 (1:10,000; NB110–55288, Novus Biologics), OPA1 (1:5000; NBP1–71656 (1E8–1D9) Novus Biologicals), ZO-1 (1:100; ab96587, Abcam), Occludin (1:100; 13409–1-AP, ProteinTech), GFAP (1:500; 3670S, Cell Signaling Technology), iba1 (1:50; 43733, Genetex). Antibody targets were detected with an HRP-conjugated secondary anti-rabbit and anti-mouse. Protein levels were evaluated by the area under the curve obtained via the Compass for SW software

(version 4.0.0, Protein Simple®, Bio-techne, Minneapolis, MN). Relative protein expression was calculated by protein peak intensity (area under the curve) divided by the Total Protein loaded as per the manufacturer. Representative computer-generated pseudo-blots are presented throughout the figures where applicable (Protein Simple®, Bio-techne, Minneapolis, MN).

2.6. Two-photon laser scanning microscopy

C57BL/6J mice from both injured (rmTBI) and uninjured cohorts (SHAM) were assessed using two-photon laser scanning microscopy. SHAM and rmTBI mice were anesthetized at 3% isoflurane and maintained at 1% for image acquisition. A thin longitudinal incision was made across the scalp in the midline stretching from the neck to the front of the head. A thin-skull preparation was done to ensure clear evaluation of the cortical vessels during image acquisition. The thin-skull procedure produced a circular cranial window ~2 mm from the bregma and 2 mm from the centerline of the skull. The surgically prepared mice were then visualized via the Zeiss LSM 510 multi-photon microscope. Mice were monitored via rectal probe and maintained at 37 °C via heating pad. Mice were injected with the following dyes via tail vein injection: fluorescein isothiocyanate-dextran (FITC) (0.2 mg/kg Cat. no. FD2000S, MilliporeSigma) to visualize red blood cells and micro-vessels and acridine orange (7 mg/kg Cat. no. 318337, MilliporeSigma) to visualize leukocytes (Cahoon et al., 2014), (Byvaltsev et al., 2019), (Lin et al., 2010), (R. H. Lee et al., 2017). For BBB leakage studies, 40 kDa FITC-dextran (Nyul-Toth et al., 2021) was injected into the tail vein to measure fluorescent intensity in the cerebral vessel and the neighboring perivascular space.

Only cortical blood vessels with a diameter of ~10–20 μm were analyzed with a 20 X objective. A total of ~3–4 linescans were acquired for each mouse. The slope was calculated for each linescan using ImageJ software and the average red blood cell velocity (labelled with FITC, a surrogate measurement for CBF) (Lin et al., 2010) or leukocyte (labelled with acridine orange) speed was measured (Lagrange et al., 2018). Whisker-barrel stimulation was produced by a motorized rotating device with a “flag-like” shape attached to the motor that was placed perpendicular to the mouse vibrissae rotating at 4 Hz for 30 s (Rodgers et al., 2006). Whisker-barrel stimulation was implemented on SHAM, SHAM + PRMT7-AAV, 3 days after rmTBI, and 3 days after rmTBI + PRMT7-AAV, while implementing two-photon microscopy imaging of cortical microvessels in real-time.

2.7. Seahorse XFe24 analyzer (mitochondrial bioenergetics)

Mitochondrial bioenergetics (oxygen consumption rate, OCR) of CA1 hippocampal tissue slices were analyzed via Seahorse XFe24 Analyzer (Agilent Technologies, Santa Clara, CA). SHAM and rmTBI mice were anesthetized with 4% isoflurane to enable removal of the brain tissue (cortex and hippocampus) at the end-point (3 days post-rmTBI). Murine brains were then placed into artificial cerebral spinal fluid buffer (aCSF). aCSF mixture consisted of the following: [120 mM NaCl (Cat. No. S7653), 3.5 mM KCl (Cat. No. P9333), 1.3 mM $CaCl_2$ (Cat. No. C1016), 1 mM $MgCl_2$ hexahydrate (Cat. No. M9272), 0.4 mM KH_2PO_4 (Cat. No. P5655), 5 mM HEPES (Cat. No. H7006), 10 mM glucose (Cat. No. G7528), and 1 mg/ml of bovine serum albumin, at a 7.4 pH at 4 °C (MilliporeSigma, Burlington, MA)]. Mouse brains were sliced into 200 μm corona sections with Leica VT1000E vibratome while

submerged in aCSF at 4 °C, transferred to aCSF at 20 °C. A 1-mm biopsy punch (Sklar Instruments; 96–0912) of the CA1 region of the hippocampus was placed independently into the wells of the Seahorse XFe24 Islet Capture Microplate (Cat. No. 103518–100; Agilent Technologies, Santa Clara, CA) containing 700 μl of aCSF. Once plated into wells, tissue slices were incubated in a step-wise method within the first 30 min to reach room temperature followed by 1 h at 37 °C, as suggested by the standard Agilent Technologies protocol. OCR measurements are made temporally at both basal levels and following each drug administration. OCR measurements were performed at the following time-points: basal conditions with aCSF media (to maintain tissue viability), 20 μg/ml oligomycin (ATP-synthase inhibitor, Cat. No. O4876), 10 μM carbonyl cyanide 4-(trifluoromethoxy) phenylhydrazone (FCCP, a mitochondrial uncoupler, Cat. No. C2920), and 20 μM antimycin A (a complex III inhibitor, Cat No. A8674 MilliporeSigma (MilliporeSigma, Burlington, MA). Upon completion, the following OCR measurements are generated: ATP production, ATP-linked respiration, maximal respiration, and reserve capacity. Mitochondrial reserve capacity was calculated by the average of tissue sections that displayed an OCR of 40–210 pmol/min (Couto et al., 2021).

2.8. Statistical analyses

A p value of ≤ 0.05 level of probability was considered significant. Results were expressed as means ± S.E.M. Statistical analysis were evaluated by Student's t-test, two-way or one-way ANOVA (Tukey's post-hoc test) as appropriate with Graph-pad Prism v.8.0.2 (San Diego, CA).

3. Results

3.1. Validation of PRMT7-AAV overexpression in vivo

Cartoon illustration of experimental design with the timeline of AAV/PHP.eB-hSYN1-GFP.mPRMT7-WPRE intravenous viral injections. Mice were injected 3–4 weeks prior to rmTBI to reach peak neuronal expression post-rmTBI (Fig. 1 A). PRMT7 protein expression was analyzed to verify overexpression in the cortex and hippocampus. There was a significant increase in PRMT7 protein expression in the (Fig. 1 B) cortex of SHAM + PRMT7-AAV injection (6.733 ± 0.6394) (Arbitrary Units, AU) relative to SHAM + non-injected mice (0.6535 ± 0.01231 AU) as well as in the (Fig. 1C) hippocampus of SHAM + PRMT7-AAV injection (7.518 ± 1.841 AU) relative to SHAM + non-injected mice (1.876 ± 0.09916 AU). In addition, mRNA expression was significantly upregulated in the (Fig. 1 D) cortex of SHAM + PRMT7-AAV injected mice (1.778 ± 0.2964 AU) relative to SHAM + non-injected mice (1.000 ± 0.03189 AU) and had a strong trending increase in the hippocampus (Fig. 1 E) of SHAM + PRMT7-AAV injected mice (1.513 ± 0.2390 AU) relative to SHAM + non-injected mice (1.003 ± 0.03924 AU) (p-value = 0.055). Results were expressed as mean ± SEM analyzed via Student's t-test.

3.2. Histological validation of PRMT7-AAV overexpression

Histological sections were qualitatively analyzed and presented with a robust increase in GFP-tagged PRMT7-AAV overexpression in the cortex and hippocampus. Vehicle treated (Lactated Ringer's) mice did not exhibit GFP expression in (Fig. 2 A) cortex (Fig. 2 B)

DAPI (blue stained) for nuclei and (Fig. 2C) composite as compared to the cortex from mice injected with AAV/PHP.eB-hSYN1-GFP.mPRMT7-WPRE vector to demonstrate the robust GFP expression (Fig. 2 D) in the cortex, (Fig. 2 E) DAPI, and (Fig. 2 F) composite image. Neuronal PRMT7-AAV overexpression in the hippocampus exhibited similar expression patterns as the cortex with no GFP in the (Fig. 2 G) vehicle-treated mice, (Fig. 2H) DAPI, (Fig. 2 I) composite image, as compared to the AAV/PHP.eB-hSYN1-GFP.mPRMT7-WPRE injected mice exhibiting robust (Fig. 2 J) GFP expression, (Fig. 2 K) DAPI for nuclei, and (Fig. 2 L) composite image.

3.3. Overexpression with PRMT7-AAV increased PRMT7 protein expression and mono-methylarginine in the cortex and hippocampus

PRMT7 and MMA protein levels were assessed in SHAM, SHAM + PRMT7-AAV mice, as well as rmTBI mice + PRMT7-AAV (3 and 7 days post-rmTBI) in whole-brain tissue. PRMT7 was significantly reduced 3 (0.8448 ± 0.02815 AU) and 7 days post-rmTBI (0.7342 ± 0.04749 AU) mice with no virus as compared to SHAM (1.000 ± 0.02628 AU) mice with no virus (Fig. 3 A). Mono-methylarginine (MMA, PRMT7 end-product) was also reduced 3 (0.5328 ± 0.1399 AU) and 7 days (0.4897 ± 0.09024 AU) with no virus as compared to SHAM (1.032 ± 0.1572 AU) (Fig. 3 B) with no virus. PRMT7-AAV overexpressed mice had a significant upregulation in PRMT7 protein levels at 3 (8.767 ± 1.588 AU) and 7 days (9.477 ± 1.779 AU) relative to SHAM (no virus) (1.000 ± 0.02628 AU) (Fig. 3 C). In addition, there was a significant increase in MMA production with PRMT7-AAV overexpression at 3 (2.239 ± 0.4482 AU) and 7 days (2.752 ± 0.4820 AU) post-rmTBI relative to SHAM (no virus) (0.7647 ± 0.06188 AU) (Fig. 3 D). In Figs. 3 C & D, all data were calculated based on SHAM group represented by a solid black line in the bar graph(s). Results were expressed as mean ± SEM analyzed via one-way ANOVA with Tukey's *post-hoc* test.

3.4. PRMT7-AAV overexpression prevented neurovascular uncoupling and cerebral blood flow derangements 3 days post-rmTBI

We investigated neurovascular coupling via whisker-barrel stimulation (4 Hz, 30 s) in conjunction with two-photon laser scanning microscopy (Fig. 4 A) by measuring cortical microvessel reactivity (Summers et al., 2017), (Lecrux et al., 2017), (Kheradpezhouh et al., 2017), (Latimer et al., 2019). Red blood cell velocity and vessel diameters were analyzed via two-photon laser scanning microscopy in SHAM, rmTBI, and PRMT7-AAV overexpressed mice before and after whisker-barrel stimulation with representative images of each group shown in Fig. 4 B. Blood vessel diameters were analyzed to suggest a marked decrease in diameter 3 days post-rmTBI (− 2.129 ± 1.581%) relative to SHAM (1.570 ± 0.6167%) (p = 0.0621), followed by restoration 3 days post-rmTBI (1.621 ± 0.8283%) in PRMT7-AAV overexpressed mice relative to 3 day rmTBI mice with no virus (p = 0.0606) (Fig. 4 C). In addition, there was a significant decrease in red blood cell velocity at 3 days post-rmTBI (2.560 ± 0.4005 mm/s) relative to SHAM (5.392 ± 0.4662 mm/s), followed by restoration at 3 days (6.490 ± 0.8900 mm/s) in PRMT7-AAV overexpressed mice relative to 3 days rmTBI mice with no virus (Fig. 4 D). Results were expressed as mean ± SEM analyzed via one-way ANOVA with Tukey's *post-hoc* test.

3.5. PRMT7-AAV overexpression prevented blood-brain barrier leakage 3 days post-rmTBI in C57BL/6J mice

Mice were intravenously injected with (40 kDa) FITC-dextran to assess the degree of blood-brain barrier leakage (Nyul-Toth et al., 2021) post-rmTBI relative to SHAM and PRMT7-AAV overexpressed mice (Fig. 5 A). Representative images of cortical blood vessels are presented at baseline and 30 min after in each experimental group (Fig. 5 B). There was a significant increase in BBB leakage at 3 days post-rmTBI (39.21 ± 4.661%) (represented by % change in extravascular FITC) relative to SHAM (17.62 ± 3.335%) followed by restoration to nominal levels at 3 days post-rmTBI (4.730 ± 4.927%) in PRMT7-AAV overexpressed mice relative to 3 days post-rmTBI mice with no virus (Fig. 5 C). There was also a significant difference in FITC extravasation between 3 days post-rmTBI (39.21 ± 4.661%) mice and SHAM + PRMT7-AAV (1.928 ± 7.309%) overexpressed mice (Fig. 5 C). Results were expressed as mean ± SEM analyzed via one-way ANOVA with Tukey's *post-hoc* test.

3.6. PRMT 7-AAV overexpression enhanced blood-brain barrier junctional proteins post-rmTBI

BBB tight junction proteins occludin and ZO-1 were investigated to assess BBB leakage in the cortex and hippocampus. In the cortex, occludin protein expression was decreased at 3 days (0.514 ± 0.162 AU ($p = 0.0925$) and 7 days (0.559 ± 0.138 AU) post-rmTBI relative to SHAM (1.00 ± 0.065 AU) (Fig. 6 A) followed by a significant upregulation in occludin protein levels in PRMT7-AAV overexpressed mice at 3 (1.407 ± 0.123 AU) and 7 days (1.207 ± 0.162 AU) relative to rmTBI mice with no virus in the cortex, respectively (Fig. 6 A). There were no significant changes observed in ZO-1 protein levels within the cortex (Fig. 6 B). In addition, there were no significant changes in occludin protein levels in the hippocampus (Fig. 6 C) however, there was a significant upregulation of ZO-1 protein at 3 days post-rmTBI (1.310 ± 0.087 AU) in the hippocampus (no virus) (Fig. 6 D) relative to sham (1.00 ± 0.066 AU) (no virus). Results were expressed as mean ± SEM analyzed via two-way ANOVA with Tukey's *post-hoc* test.

3.7. PRMT 7-AAV overexpression enhanced leukocyte rolling velocity

Leukocyte rolling velocity was assessed as area traveled over time via intravenous injection of acridine orange using two-photon scanning microscopy. Representative images of leukocytes traveling through the blood vessel (Fig. 7 A) as well as leukocyte line-scan images (Fig. 7 B). There was a significant decrease in leukocyte rolling velocity at 3 days post-rmTBI (3.138 ± 0.5188 mm/s) relative to SHAM (10.12 ± 1.093 mm/s) (Fig. 7 C). PRMT7-AAV overexpression enhanced leukocyte rolling velocity 3 days post-rmTBI (9.730 ± 1.067 mm/s) relative to 3 days post-rmTBI mice with no virus (Fig. 7 C). Results were expressed as mean ± SEM analyzed via one-way ANOVA with Tukey's *post-hoc* test.

3.8. PRMT7-AAV overexpression attenuated gliosis in hippocampus

Astrocyte marker and astrogliosis indicator, glial fibrillary acidic protein (GFAP) was probed in the hippocampus, as well as the microglia marker and microgliosis indicator ionized calcium binding adaptor molecule 1 (iba1). Mouse hippocampal GFAP was

enhanced 3 days post-rmTBI v. SHAM (although not significant) but decreased in PRMT7-AAV overexpressed mice at 3 days post-rmTBI (0.255 ± 0.056 AU) v. 3 days post-rmTBI mice with no virus (0.598 ± 0.155 AU) ($p = 0.0856$) (Fig. 8 A). Moreover, there was a time-dependent increase in hippocampal iba1 in rmTBI mice, followed by modest attenuation of iba1 protein levels at all time-points in PRMT7-AAV overexpressed mice (Fig. 8 B). Results were expressed as mean ± SEM analyzed via two-way ANOVA with Tukey's *post-hoc* test.

3.9. PRMT 7-AAV overexpression improved mitochondrial reserve capacity 3 days post-rmTBI

Oxygen consumption rates were analyzed via Seahorse XFe24 analyzer to assess mitochondrial bioenergetics *ex vivo* (Fig. 9 A). Mouse CA1 region of the hippocampus were analyzed from SHAM, SHAM + PRMT7-AAV, rmTBI, and rmTBI + PRMT7-AAV overexpressed mice. There were no changes in maximal respiration (Fig. 9 B), however, PRMT7-AAV overexpressed mice had significantly increased reserve capacity 3 days post-rmTBI (123.0 ± 3.068 AU) relative to SHAM (102.2 ± 3.039 AU), 3 days post-rmTBI (104.9 ± 4.855 AU), and SHAM + PRMT7-AAV (95.24 ± 5.468 AU) (Fig. 9 C). In addition, (Fig. 9 D) proton leak-linked respiration and (Fig. 9 E) basal respiration remained unchanged in each of the experimental groups. Moreover, there was a significant decrease in ATP-linked respiration at 3 days post-rmTBI + PRMT7-AAV (64.53 ± 0.7621 AU) relative to 3 days post-rmTBI with no virus (96.65 ± 7.487 AU) (Fig. 9 F). Lastly, ATP production was also decreased 3 days post-rmTBI (57.36 ± 1.129 AU) + PRMT7-AAV relative to 3 days post-rmTBI mice (90.50 ± 6.424 AU) with no virus (Fig. 9 G). Results were expressed as mean ± SEM analyzed via one-way ANOVA with Tukey's *post-hoc* test.

3.10. PRMT7-AAV overexpression enhanced mitochondrial fusion (OPA1) and fission (DRP1) proteins 7 days post-rmTBI

Dynamin related protein 1 (DRP1, mitochondrial fission marker) and optic atrophy 1 (OPA1, mitochondrial fusion marker) were probed in the cortex and hippocampus. This fission marker DRP1 was unchanged in the cortex (Fig. 10 A). However, the fusion marker OPA1, was significantly reduced in the cortex at 7 days post-rmTBI (0.764 ± 0.061 AU) relative to SHAM (1.00 ± 0.076 AU), followed by a significant increase at 7 days post-rmTBI (1.042 ± 0.037 AU) + PRMT7-AAV mice relative to 7 days post-rmTBI mice with no virus (Fig. 10 B). DRP1 was significantly decreased in the hippocampus 7 days post-rmTBI (0.724 ± 0.120 AU) relative to SHAM (1.00 ± 0.016 AU) and increased via PRMT7-AAV (1.073 ± 0.034 AU) relative to 7 days post-rmTBI mice with no virus (Fig. 10 C). In addition, OPA1 was also significantly reduced in the hippocampus at 7 days post-rmTBI (0.731 ± 0.101 AU) relative to SHAM (1.000 ± 0.049 AU) but enhanced in PRMT7-AAV mice at 7 day (1.053 ± 0.042 AU) post-rmTBI relative to 7 days post-rmTBI with no virus (Fig. 10 D). Results were expressed as mean ± SEM analyzed via two-way ANOVA with Tukey's *post-hoc* test.

4. Discussion

The goals of this study were to determine if overexpression of PRMT7-AAV *in vivo* could attenuate CBF derangements, BBB permeability/leakage, and mitochondrial dysfunction as our three-hit rmTBI paradigm contributed to decreased PRMT7 protein levels and activity

(through MMA protein analyses) post-rmTBI (Figs. 3 A, B). PRMT7 has been implicated in several clinical diseases ranging from cancer, cardiovascular disease, to developmental disorders and neurological function (Oksa et al., 2022), (C. Liu et al., 2022), (L. Liu et al., 2021), (Poquerusse et al., 2022), (Agolini et al., 2018), (S. Y. Lee et al., 2020), (W. Zhang et al., 2021), (S. Y. Lee et al., 2019), (Ma et al., 2022), (Fiorica and Wheeler, 2019), (Ahn et al., 2022). Here, we show overexpression of PRMT7-AAV via AAV/PHP.eB-hSYN1-GFP.mPRMT7-WPRE, as observed by the significant increase in PRMT7 protein expression in both the cortex and hippocampus (Figs. 1 B, C), and positive PRMT7-AAV GFP-tagged histological sections (Figs. 2 A–L). Following validation of PRMT7-AAV overexpression in our SHAM mice, we tested the levels of PRMT7 and its end-product MMA at 3 and 7 days post-rmTBI in PRMT7-AAV mice and found PRMT7 protein levels to be significantly enhanced (Fig. 3 C), as well as it's end-product MMA as a measure of PRMT7 activity (Fig. 3 D). Neuronal overexpression of PRMT7-AAV *in vivo* prevented neurovascular uncoupling (Fig. 4), mitigated BBB permeability/leakage (Figs. 5–6), enhanced leukocyte rolling velocities (Fig. 7), improved gliosis (Fig. 8), and restored mitochondrial bioenergetics/dynamics (Figs. 9–10). The upregulation of PRMT7 protein and activity after injury signifies a potential role in which PRMT7 can prevent injury in our model of rmTBI. Our data supports a functional role in which neuronal overexpression of PRMT7-AAV is involved in a protective capacity in the pathological progression of rmTBI.

TBI leads to a multitude of pathologies that originate from the initial (For interpretation of the references to colour in this figure legend, the reader is referred to the web version of this article.) impact as well as a cascade of injuries that ensue, also known as secondary injury (McKee and Daneshvar, 2015), (Namjoshi et al., 2014), (Wilson et al., 2017). Secondary injuries involve damage to tissue and cells that regulate CBF, astrocytes, endothelial cells, pericytes as well as the integrity of the BBB (Toth et al., 2016). CBF derangements are well-documented in both pre-clinical studies of murine models as well as in human TBI patients (Vedung et al., 2022), (L. Xu et al., 2021), (Toth et al., 2016), (Ware et al., 2020), (Clark et al., 2021), (Sandsmark et al., 2019), (Kenney et al., 2016). CBF dynamics are regulated post injury by complex systems such as autoregulation and neurovascular coupling (Toth et al., 2016), (Vedung et al., 2022). CBF autoregulation involves a combination of pressure-induced myogenic responses, regional metabolic demand, and sympathetic mechanisms (Das et al., 2022), (Stephens et al., 2018), (Li et al., 2020). This maintenance ensures a continuous supply of oxygen and nutrients to meet the dynamic requirements of cerebral tissue to prevent instances of hypoxia and ischemia (Toth et al., 2016), (Vedung et al., 2022). Mechanisms in place include neurovascular coupling to meet energy requirements of active neurons and/or glial cells as well as pressure-induced vasomotor auto-regulation to modulate the diameter of cerebral resistance vessels (Toth et al., 2016), (Vedung et al., 2022).

A major advantage of the rmTBI via CHIMERA is the ability to observe cerebral vascular deficits because it does not cause severe brain hemorrhage found in other models of TBI [controlled cortical impact (Muller et al., 2021) and fluid percussion injury, (Katz and Molina, 2018)]. Since contrast dyes such as FITC are introduced into the animal for vascular imaging, brain hemorrhage-induced bleeding by invasive models of TBI can prevent accurate imaging and analysis and is one of the main drawbacks of other TBI models. Therefore, we used CHIMERA coupled with whisker-barrel stimulation and two-

photon laser scanning microscopy to measure cortical microvessel diameters and red blood cell speed (a surrogate measure of CBF as published previously from our lab, (Lin et al., 2010) to suggest reduced cortical RBC velocity and microvessel diameters 3 days post-rmTBI. This was reversed (enhanced RBC and microvessel diameters) in the presence of PRMT7-AAV to suggest restoration of neurovascular coupling. This is further corroborated with clinical findings to suggest increased injury severity and persistent functional deficits post-injury is correlated with an overall decrease in CBF (Ware et al., 2020), (Vedung et al., 2022). Given the role of PRMT7 in cell stress responses (Szewczyk et al., 2020), (Haghandish et al., 2019) as well as its role in DNA damage repair (Karkhanis et al., 2012), (A. Jeong et al., 2022), (Brobbey et al., 2022), PRMT7 could elicit protective effects by cellular preconditioning (Dave et al., 2001), (Koch et al., 2012), as well as a response to the injury via cell stress response pathways.

Our model of rmTBI also led to enhanced BBB permeability (more leakage), decreased junctional protein expression and leukocyte rolling velocity post-rmTBI (George et al., 2022), (Szarka et al., 2019), (Huang et al., 2023). However, mice overexpressed with PRMT7-AAV prevented BBB leakage, enhanced junctional protein expression, and increased leukocyte rolling velocities, similar to SHAM levels. Although still controversial, faster leukocyte velocities may be more beneficial to counteract inflammation and clear the inflammatory response (Schnoor et al., 2015), (Tsujikawa and Ogura, 2012), while slower circulating leukocytes can penetrate neighboring tissues triggering inflammation (Sundd et al., 2011),(Kadono et al., 2002). Moreover, PRMT7-AAV overexpression modestly reduced reactive astrogliosis via decreased GFAP levels, and improved microgliosis as evident from the reduced iba1 protein expression. Though still controversial, some reports have suggested elevated astrogliosis acutely at 1, 2 and 7 days post-rmTBI (Chen et al., 2017), (Haber et al., 2017), (Namjoshi et al., 2017), while others observed no changes (Nolan et al., 2018), (Gangolli et al., 2019). This can be attributed to the heterogeneity of various parameters of rmTBI, such as joules of kinetic energy, time intervals between hits, number of rmTBI hits, strain and age of mice in the experiments. Moreover, primary TBI injury can lead to BBB disruption and subsequent leakage of serum proteins to induce subsequent neuroinflammation (Babcock et al., 2022), (George et al., 2022), (Michinaga and Koyama, 2019). In turn, this process leads to enhanced BBB permeability to contribute to a cascade of secondary injury (Babcock et al., 2022), (George et al., 2022), (Michinaga and Koyama, 2019). BBB leakage post-injury could enable homeostatic leukocyte velocities, as there would be less surface adhesion molecules for leukocytes to adhere to for diapedesis and subsequent neuroinflammation (Y. W. Liu et al., 2018).

In addition, PRMT7-AAV overexpression improved mitochondrial bioenergetics by significantly increasing reserve capacity, decreasing ATP production, and ATP-linked respiration in 3 days rmTBI mice v. 3 days rmTBI with no virus. Previous reports suggest PRMT7 deficiency has been linked to reduced oxidative metabolism (H. J. Jeong et al., 2016), supporting the notion that PRMT7 can influence mitochondrial function. In addition, PRMT7 has been reported to be activated upon cellular stress such as oxidative stress and endoplasmic reticulum stress, which occur post-TBI (Haghandish et al., 2019). This can explain, in part, why we observed functional enhancement of PRMT7 activity only after injury in our PRMT7-AAV overexpressed mouse model of rmTBI.

Altered mitochondrial bioenergetics can negatively impact the delicate process of mitochondrial fission and fusion. Mitochondrial dynamics (fission and fusion) are closely involved with the maintenance of neuronal cell survival, growth, and death (Fischer et al., 2016). Mitochondria undergo a continuous and dynamic process of dividing and fusing for the removal of damaged and/or dying mitochondria. A disturbance in this dynamic process can lead to deleterious outcomes for the mitochondrial function, especially in the context of neurons as this process is crucial in mobilizing mitochondria across great axon lengths to meet the energy demands throughout cerebral tissue; (Gao et al., 2017) and can lead to excess reactive oxygen species generation, apoptosis, and poor cognitive outcome post-TBI (Song et al., 2019). Therefore, we assessed the mitochondrial master regulators of fission (DRP1) and fusion (OPA1), which were decreased at 7 days post-rmTBI and were restored with overexpression of PRMT7-AAV. Our data suggest restoration of mitochondrial dynamics and bioenergetics upon PRMT7-AAV overexpression post-rmTBI. The restoration of the BBB, CBF derangements, and leukocyte rolling velocities suggest decreased cerebral energy demand in response to attenuated injury post-rmTBI, which can improve mitochondrial function.

5. Conclusion

Endogenous PRMT7 deficiency and activity in our model of rmTBI exacerbated CBF derangements, BBB permeability, and mitochondrial dysfunction. *In vivo* PRMT7-AAV overexpression was able to mitigate the above rmTBI pathologies, highlighting the potential protective role in neurodegeneration post-rmTBI. To our knowledge, this is the first report that describes a protective and functional role of PRMT7 within rmTBI murine models.

Funding sources

Funding and support for this study are from the NIH/NINDS 5R01NS096225–05, 1R01NS126273–01, the AHA 22PRE903112, 22TPA970253, 19CDA3466032, 21CDA856826, and the Louisiana State University Research Council, the Joanna G. Magale Foundation.

Data availability

Data will be made available on request.

Abbreviations:

rmTBI	repetitive and mild traumatic brain injury
PRMT7	protein arginine methyltransferase 7
MMA	mono-methylarginine
BBB	blood-brain barrier
CBF	cerebral blood flow
RBC	red blood cell
CHIMERA	closed head impact of engineered rotational acceleration

References

Acosta CH, Clemons GA, Citadin CT, Carr WC, Udo MSB, Tesic V, Lin HW, 2023. A role for protein arginine methyltransferase 7 in repetitive and mild traumatic brain injury. Neurochem. Int 105524 10.1016/j.neuint.2023.105524.

Agolini E, Dentici ML, Bellacchio E, Alesi V, Radio FC, Torella A, Novelli A, 2018. Expanding the clinical and molecular spectrum of PRMT7 mutations: 3 additional patients and review. Clin. Genet 93 (3), 675–681. 10.1111/cge.13137. [PubMed: 28902392]

Ahn BY, Jeong MH, Pyun JH, Jeong HJ, Vuong TA, Bae JH, Kang JS, 2022. PRMT7 ablation in cardiomyocytes causes cardiac hypertrophy and fibrosis through beta-catenin dysregulation. Cell. Mol. Life Sci 79 (2), 99. 10.1007/s00018-021-04097-x. [PubMed: 35089423]

Babcock KJ, Abdolmohammadi B, Kiernan PT, Mahar I, Cherry JD, Alvarez VE, Huber BR, 2022. Interface astrogliosis in contact sport head impacts and military blast exposure. Acta Neuropathol. Commun 10 (1), 52. 10.1186/s40478-022-01358-z. [PubMed: 35418116]

Balasubramanian N, Jadhav G, Sakharkar AJ, 2021. Repeated mild traumatic brain injuries perturb the mitochondrial biogenesis via DNA methylation in the hippocampus of rat. Mitochondrion 61, 11–24. 10.1016/j.mito.2021.09.001. [PubMed: 34508891]

Brobbey C, Liu L, Yin S, Gan W, 2022. The role of protein arginine methyltransferases in DNA damage response. Int. J. Mol. Sci 23 (17) 10.3390/ijms23179780.

Busto R, Globus MY, Dietrich WD, Martinez E, Valdes I, Ginsberg MD, 1989. Effect of mild hypothermia on ischemia-induced release of neurotransmitters and free fatty acids in rat brain. Stroke 20 (7), 904–910. 10.1161/01.str.20.7.904. [PubMed: 2568705]

Byvaltsev VA, Bardonova LA, Onaka NR, Polkin RA, Ochkal SV, Shepelev VV, Potapov AA, 2019. Acridine Orange: a review of novel applications for surgical Cancer imaging and therapy. Front. Oncol 9, 925. 10.3389/fonc.2019.00925. [PubMed: 31612102]

Cahoon JM, Olson PR, Nielson S, Miya TR, Bankhead P, McGeown JG, Ambati BK, 2014. Acridine orange leukocyte fluorography in mice. Exp. Eye Res 120, 15–19. 10.1016/j.exer.2013.12.002. [PubMed: 24333760]

Cash A, Theus MH, 2020. Mechanisms of blood-brain barrier dysfunction in traumatic brain injury. Int. J. Mol. Sci 21 (9) 10.3390/ijms21093344.

Chen H, Desai A, Kim HY, 2017. Repetitive closed-head impact model of engineered rotational acceleration induces long-term cognitive impairments with persistent Astrogliosis and microgliosis in mice. J. Neurotrauma 34 (14), 2291–2302. 10.1089/neu.2016.4870. [PubMed: 28288551]

Cheng WH, Martens KM, Bashir A, Cheung H, Stukas S, Gibbs E, Wellington CL, 2019. CHIMERA repetitive mild traumatic brain injury induces chronic behavioural and neuropathological phenotypes in wild-type and APP/PS1 mice. Alzheimers Res. Ther 11 (1), 6. 10.1186/s13195-018-0461-0. [PubMed: 30636629]

Clark AL, Weigand AJ, Bangen KJ, Merritt VC, Bondi MW, Delano-Wood L, 2021. Repetitive mTBI is associated with age-related reductions in cerebral blood flow but not cortical thickness. J. Cereb. Blood Flow Metab 41 (2), 431–444. 10.1177/0271678X19897443. [PubMed: 32248731]

Couto ESA, Wu CY, Clemons GA, Acosta CH, Chen CT, Possoit HE, Lin HW, 2021. Protein arginine methyltransferase 8 modulates mitochondrial bioenergetics and neuroinflammation after hypoxic stress. J. Neurochem 159 (4), 742–761. 10.1111/jnc.15462. [PubMed: 34216036]

Das AS, Vicenty-Padilla JC, Chua MMJ, Jeelani Y, Snider SB, Regenhardt RW, Izzy S, 2022. Cerebrovascular injuries in traumatic brain injury. Clin. Neurol. Neurosurg 223, 107479 10.1016/j.clineuro.2022.107479.

Dave KR, Saul I, Busto R, Ginsberg MD, Sick TJ, Perez-Pinzon MA, 2001. Ischemic preconditioning preserves mitochondrial function after global cerebral ischemia in rat hippocampus. J. Cereb. Blood Flow Metab 21 (12), 1401–1410. 10.1097/00004647-200112000-00004. [PubMed: 11740201]

Demers-Marcil S, Coles JP, 2022. Cerebral metabolic derangements following traumatic brain injury. Curr. Opin. Anaesthesiol 35 (5), 562–569. 10.1097/ACO.0000000000001183. [PubMed: 35943124]

Dietrich WD, Bramlett HM, 2010. The evidence for hypothermia as a neuroprotectant in traumatic brain injury. Neurotherapeutics 7 (1), 43–50. 10.1016/j.nurt.2009.10.015. [PubMed: 20129496]

Du M, Wu C, Yu R, Cheng Y, Tang Z, Wu B, Liao ZB, 2022. A novel circular RNA, circIgfbp2, links neural plasticity and anxiety through targeting mitochondrial dysfunction and oxidative stress-induced synapse dysfunction after traumatic brain injury. Mol. Psychiatry 27 (11), 4575–4589. 10.1038/s41380-022-01711-7. [PubMed: 35918398]

Fiorica PN, Wheeler HE, 2019. Transcriptome association studies of neuropsychiatric traits in African Americans implicate PRMT7 in schizophrenia. PeerJ 7, e7778. 10.7717/peerj.7778.

Fischer TD, Hylin MJ, Zhao J, Moore AN, Waxham MN, Dash PK, 2016. Altered mitochondrial dynamics and TBI pathophysiology. Front. Syst. Neurosci 10, 29. 10.3389/fnsys.2016.00029. [PubMed: 27065821]

Gangolli M, Benetatos J, Esparza TJ, Fountain EM, Seneviratne S, Brody DL, 2019. Repetitive concussive and subconcussive injury in a human tau mouse model results in chronic cognitive dysfunction and disruption of white matter tracts, but not tau pathology. J. Neurotrauma 36 (5), 735–755. 10.1089/neu.2018.5700. [PubMed: 30136628]

Gao J, Wang L, Liu J, Xie F, Su B, Wang X, 2017. Abnormalities of mitochondrial dynamics in neurodegenerative diseases. Antioxidants (Basel) 6 (2). 10.3390/antiox6020025.

George KK, Heithoff BP, Shandra O, Robel S, 2022. Mild traumatic brain injury/concussion initiates an atypical astrocyte response caused by blood-brain barrier dysfunction. J. Neurotrauma 39 (1–2), 211–226. 10.1089/neu.2021.0204. [PubMed: 34806422]

Haber M, Hutchinson EB, Sadeghi N, Cheng WH, Namjoshi D, Cripton P, Pierpaoli C, 2017. Defining an analytic framework to evaluate quantitative MRI markers of traumatic axonal injury: preliminary results in a mouse closed head injury model. eNeuro 4 (5). 10.1523/ENEURO.0164-17.2017.

Haghandish N, Baldwin RM, Morettin A, Dawit HT, Adhikary H, Masson JY, Cote J, 2019. PRMT7 methylates eukaryotic translation initiation factor 2alpha and regulates its role in stress granule formation. Mol. Biol. Cell 30 (6), 778–793. 10.1091/mbc.E18-05-0330. [PubMed: 30699057]

Hartl R, Medary MB, Ruge M, Arfors KE, Ghajar J, 1997. Early white blood cell dynamics after traumatic brain injury: effects on the cerebral microcirculation. J. Cereb. Blood Flow Metab 17 (11), 1210–1220. 10.1097/00004647-199711000-00010. [PubMed: 9390653]

Howe EI, Zeldovich M, Andelic N, von Steinbuechel N, Fure SCR, Borgen IMH, investigators., 2022. Rehabilitation and outcomes after complicated vs uncomplicated mild TBI: results from the CENTER-TBI study. BMC Health Serv. Res 22 (1), 1536. 10.1186/s12913-022-08908-0. [PubMed: 36527074]

Huang J, Zhu H, Yu P, Ma Y, Gong J, Fu Y, Jiang G, 2023. Recombinant high-density lipoprotein boosts the therapeutic efficacy of mild hypothermia in traumatic brain injury. ACS Appl. Mater. Interfaces 15 (1), 26–38. 10.1021/acsami.2c02940. [PubMed: 35833835]

Jeong HJ, Lee HJ, Vuong TA, Choi KS, Choi D, Koo SH, Kang JS, 2016. Prmt7 deficiency causes reduced skeletal muscle oxidative metabolism and age-related obesity. Diabetes 65 (7), 1868–1882. 10.2337/db15-1500. [PubMed: 27207521]

Jeong A, Cho Y, Cho M, Bae GU, Song DG, Kim SN, Kim YK, 2022. PRMT7 inhibitor SGC8158 enhances doxorubicin-induced DNA damage and its cytotoxicity. Int. J. Mol. Sci 23 (20) 10.3390/ijms232012323.

Johnson VE, Stewart JE, Begbie FD, Trojanowski JQ, Smith DH, Stewart W, 2013. Inflammation and white matter degeneration persist for years after a single traumatic brain injury. Brain 136 (Pt 1), 28–42. 10.1093/brain/aws322. [PubMed: 23365092]

Kadono T, Venturi GM, Steeber DA, Tedder TF, 2002. Leukocyte rolling velocities and migration are optimized by cooperative L-selectin and intercellular adhesion molecule-1 functions. J. Immunol 169 (8), 4542–4550. 10.4049/jimmunol.169.8.4542. [PubMed: 12370391]

Karkhanis V, Wang L, Tae S, Hu YJ, Imbalzano AN, Sif S, 2012. Protein arginine methyltransferase 7 regulates cellular response to DNA damage by methylating promoter histones H2A and H4 of the polymerase delta catalytic subunit gene, POLD1. J. Biol. Chem 287 (35), 29801–29814. 10.1074/jbc.M112.378281. [PubMed: 22761421]

Katz PS, Molina PE, 2018. A lateral fluid percussion injury model for studying traumatic brain injury in rats. Methods Mol. Biol 1717, 27–36. 10.1007/978-1-4939-7526-6_3.

Kenney K, Amyot F, Haber M, Pronger A, Bogoslovsky T, Moore C, Diaz-Arrastia R, 2016. Cerebral vascular injury in traumatic brain injury. Exp. Neurol 275 (Pt 3), 353–366. 10.1016/j.expneurol.2015.05.019. [PubMed: 26048614]

Khacho M, Clark A, Svoboda DS, MacLaurin JG, Lagace DC, Park DS, Slack RS, 2017. Mitochondrial dysfunction underlies cognitive defects as a result of neural stem cell depletion and impaired neurogenesis. Hum. Mol. Genet 26 (17), 3327–3341. 10.1093/hmg/ddx217. [PubMed: 28595361]

Kheradpezhouh E, Adibi M, Arabzadeh E, 2017. Response dynamics of rat barrel cortex neurons to repeated sensory stimulation. Sci. Rep 7 (1), 11445. 10.1038/s41598-017-11477-6. [PubMed: 28904406]

Kim S, Han SC, Gallan AJ, Hayes JP, 2017. Neurometabolic indicators of mitochondrial dysfunction in repetitive mild traumatic brain injury. Concussion 2 (3). 10.2217/cnc-2017-0013. CNC48.

Koch S, Sacco RL, Perez-Pinzon MA, 2012. Preconditioning the brain: moving on to the next frontier of neurotherapeutics. Stroke 43 (6), 1455–1457. 10.1161/STROKEAHA.111.646919. [PubMed: 22461331]

Lagrange J, Kossmann S, Kiouptsi K, Wenzel P, 2018. Visualizing leukocyte rolling and adhesion in angiotensin II-infused mice: techniques and pitfalls. J. Vis. Exp 131 10.3791/56948.

Latimer KW, Barbera D, Sokoletsky M, Awwad B, Katz Y, Nelken I, Priebe NJ, 2019. Multiple timescales account for adaptive responses across sensory cortices. J. Neurosci 39 (50), 10019–10033. 10.1523/JNEUROSCI.1642-19.2019. [PubMed: 31662427]

Lecrux C, Sandoe CH, Neupane S, Kropf P, Toussay X, Tong XK, Hamel E, 2017. Impact of altered cholinergic tones on the neurovascular coupling response to whisker stimulation. J. Neurosci 37 (6), 1518–1531. 10.1523/JNEUROSCI.1784-16.2016. [PubMed: 28069927]

Lee RH, Couto ESA, Lerner FM, Wilkins CS, Valido SE, Klein DD, Lin HW, 2017. Interruption of perivascular sympathetic nerves of cerebral arteries offers neuroprotection against ischemia. Am. J. Physiol. Heart Circ. Physiol 312 (1), H182–H188. 10.1152/ajpheart.00482.2016. [PubMed: 27864234]

Lee SY, Vuong TA, Wen X, Jeong HJ, So HK, Kwon I, Cho H, 2019. Methylation determines the extracellular calcium sensitivity of the leak channel NALCN in hippocampal dentate granule cells. Exp. Mol. Med 51 (10), 1–14. 10.1038/s12276-019-0325-0.

Lee SY, Vuong TA, So HK, Kim HJ, Kim YB, Kang JS, Cho H, 2020. PRMT7 deficiency causes dysregulation of the HCN channels in the CA1 pyramidal cells and impairment of social behaviors. Exp. Mol. Med 52 (4), 604–614. 10.1038/s12276-020-0417-x. [PubMed: 32269286]

Li F, Lu L, Shang S, Chen H, Wang P, Haidari NA, Yin X, 2020. Cerebral blood flow and its connectivity deficits in mild traumatic brain injury at the acute stage. Neural. Plast 2020, 2174371. 10.1155/2020/2174371.

Lin HW, Defazio RA, Della-Morte D, Thompson JW, Narayanan SV, Raval AP, Perez-Pinzon MA, 2010. Derangements of post-ischemic cerebral blood flow by protein kinase C delta. Neuroscience 171 (2), 566–576. 10.1016/j.neuroscience.2010.08.058. [PubMed: 20813167]

Liu YW, Li S, Dai SS, 2018. Neutrophils in traumatic brain injury (TBI): friend or foe? J. Neuroinflammation 15 (1), 146. 10.1186/s12974-018-1173-x. [PubMed: 29776443]

Liu L, Zhang X, Ding H, Liu X, Cao D, Liu Y, Lu J, 2021. Arginine and lysine methylation of MRPS23 promotes breast cancer metastasis through regulating OXPHOS. Oncogene 40 (20), 3548–3563. 10.1038/s41388-021-01785-7. [PubMed: 33927350]

Liu C, Zou W, Nie D, Li S, Duan C, Zhou M, Pan J, 2022. Loss of PRMT7 reprograms glycine metabolism to selectively eradicate leukemia stem cells in CML. Cell Metab. 34 (6), 818–835 e817. 10.1016/j.cmet.2022.04.004. [PubMed: 35508169]

Ma T, Li L, Chen R, Yang L, Sun H, Du S, Liu JY, 2022. Protein arginine methyltransferase 7 modulates neuronal excitability by interacting with NaV1.9. Pain 163 (4), 753–764. 10.1097/j.pain.0000000000002421. [PubMed: 34326297]

McKee AC, Daneshvar DH, 2015. The neuropathology of traumatic brain injury. Handb. Clin. Neurol 127, 45–66. 10.1016/B978-0-444-52892-6.00004-0. [PubMed: 25702209]

Michinaga S, Koyama Y, 2019. Dual roles of astrocyte-derived factors in regulation of blood-brain barrier function after brain damage. Int. J. Mol. Sci 20 (3) 10.3390/ijms20030571.

Moore HL, Blain AP, Turnbull DM, Gorman GS, 2020. Systematic review of cognitive deficits in adult mitochondrial disease. Eur. J. Neurol 27 (1), 3–17. 10.1111/ene.14068. [PubMed: 31448495]

Moro F, Lisi I, Tolomeo D, Vegliante G, Pascente R, Mazzone E, Zanier ER, 2022. Acute blood levels of neurofilament light indicate one-year white matter pathology and functional impairment in repetitive mild traumatic brain injured mice. J. Neurotrauma 10.1089/neu.2022.0252.

Muller CR, Courelli V, Lucas A, Williams AT, Li JB, Dos Santos F, Cabrales P, 2021. Resuscitation from hemorrhagic shock after traumatic brain injury with polymerized hemoglobin. Sci. Rep 11 (1), 2509. 10.1038/s41598-021-81717-3. [PubMed: 33510204]

Namjoshi DR, Cheng WH, McInnes KA, Martens KM, Carr M, Wilkinson A, Wellington CL, 2014. Merging pathology with biomechanics using CHIMERA (closed-head impact model of engineered rotational acceleration): a novel, surgery-free model of traumatic brain injury. Mol. Neurodegener 9, 55. 10.1186/1750-1326-9-55. [PubMed: 25443413]

Namjoshi DR, Cheng WH, Bashir A, Wilkinson A, Stukas S, Martens KM, Wellington CL, 2017. Defining the biomechanical and biological threshold of murine mild traumatic brain injury using CHIMERA (closed head impact model of engineered rotational acceleration). Exp. Neurol 292, 80–91. 10.1016/j.expneurol.2017.03.003. [PubMed: 28274861]

Narayan C, Kumar A, 2012. Constitutive over expression of IL-1beta, IL-6, NF-kappaB, and Stat3 is a potential cause of lung tumorgenesis in urethane (ethyl carbamate) induced Balb/c mice. J. Carcinog 11, 9. 10.4103/1477-3163.98965. [PubMed: 22919282]

Nolan A, Hennessy E, Krukowski K, Guglielmetti C, Chaumeil MM, Sohal VS, Rosi S, 2018. Repeated mild head injury leads to wide-ranging deficits in higher-order cognitive functions associated with the prefrontal cortex. J. Neurotrauma 35 (20), 2425–2434. 10.1089/neu.2018.5731. [PubMed: 29732949]

Nyul-Toth A, Tarantini S, DelFavero J, Yan F, Balasubramanian P, Yabluchanskiy A, Ungvari Z, 2021. Demonstration of age-related blood-brain barrier disruption and cerebromicrovascular rarefaction in mice by longitudinal intravital two-photon microscopy and optical coherence tomography. Am. J. Physiol. Heart Circ. Physiol 320 (4), H1370–H1392. 10.1152/ajpheart.00709.2020. [PubMed: 33543687]

Oksa L, Makinen A, Nikkila A, Hyvarinen N, Laukkanen S, Rokka A, Lohi O, 2022. Arginine methyltransferase PRMT7 deregulates expression of RUNX1 target genes in T-cell acute lymphoblastic leukemia. Cancers (Basel) 14 (9). 10.3390/cancers14092169.

Poquerusse J, Whitford W, Taylor J, Alburaiky S, Snell RG, Lehnert K, Jacobsen JC, 2022. Novel PRMT7 mutation in a rare case of dysmorphism and intellectual disability. J. Hum. Genet 67 (1), 19–26. 10.1038/s10038-021-00955-5. [PubMed: 34244600]

Rodgers KM, Benison AM, Barth DS, 2006. Two-dimensional coincidence detection in the vibrissa/barrel field. J. Neurophysiol 96 (4), 1981–1990. 10.1152/jn.00404.2006. [PubMed: 16790595]

Sandsmark DK, Bashir A, Wellington CL, Diaz-Arrastia R, 2019. Cerebral microvascular injury: a potentially treatable Endophenotype of traumatic brain injury-induced neurodegeneration. Neuron 103 (3), 367–379. 10.1016/j.neuron.2019.06.002. [PubMed: 31394062]

Schnoor M, Alcaide P, Voisin MB, van Buul JD, 2015. Crossing the Vascular Wall: common and unique mechanisms exploited by different leukocyte subsets during extravasation. Mediat. Inflamm 2015, 946509 10.1155/2015/946509.

Schwarzmaier SM, Kim SW, Trabold R, Plesnila N, 2010. Temporal profile of thrombogenesis in the cerebral microcirculation after traumatic brain injury in mice. J. Neurotrauma 27 (1), 121–130. 10.1089/neu.2009.1114. [PubMed: 19803784]

Schwarzmaier SM, Zimmermann R, McGarry NB, Trabold R, Kim SW, Plesnila N, 2013. In vivo temporal and spatial profile of leukocyte adhesion and migration after experimental traumatic brain injury in mice. J. Neuroinflammation 10, 32. 10.1186/1742-2094-10-32. [PubMed: 23448240]

Song Y, Li T, Liu Z, Xu Z, Zhang Z, Chi L, Liu Y, 2019. Inhibition of Drp1 after traumatic brain injury provides brain protection and improves behavioral performance in rats. Chem. Biol. Interact 304, 173–185. 10.1016/j.cbi.2019.03.013. [PubMed: 30894316]

Stephens JA, Liu P, Lu H, Suskauer SJ, 2018. Cerebral blood flow after mild traumatic brain injury: associations between symptoms and post-injury perfusion. J. Neurotrauma 35 (2), 241–248. 10.1089/neu.2017.5237. [PubMed: 28967326]

Summers PM, Hartmann DA, Hui ES, Nie X, Deardorff RL, McKinnon ET, Shih AY, 2017. Functional deficits induced by cortical microinfarcts. J. Cereb. Blood Flow Metab 37 (11), 3599–3614. 10.1177/0271678X16685573. [PubMed: 28090802]

Sun GW, Ding TY, Wang M, Hu CL, Gu JJ, Li J, Qiu T, 2022. Honokiol reduces mitochondrial dysfunction and inhibits apoptosis of nerve cells in rats with traumatic brain injury by activating the mitochondrial unfolded protein response. J. Mol. Neurosci 72 (12), 2464–2472. 10.1007/s12031-022-02089-5. [PubMed: 36508141]

Sundd P, Pospieszalska MK, Cheung LS, Konstantopoulos K, Ley K, 2011. Biomechanics of leukocyte rolling. Biorheology 48 (1), 1–35. 10.3233/BIR-2011-0579. [PubMed: 21515934]

Szarka N, Toth L, Czigler A, Kellermayer Z, Ungvari Z, Amrein K, Toth P, 2019. Single mild traumatic brain injury induces persistent disruption of the blood-brain barrier, Neuroinflammation and cognitive decline in hypertensive rats. Int. J. Mol. Sci 20 (13) 10.3390/ijms20133223.

Szewczyk MM, Ishikawa Y, Organ S, Sakai N, Li F, Halabelian L, Barsyte-Lovejoy D, 2020. Pharmacological inhibition of PRMT7 links arginine monomethylation to the cellular stress response. Nat. Commun 11 (1), 2396. 10.1038/s41467-020-16271-z. [PubMed: 32409666]

Toth P, Szarka N, Farkas E, Ezer E, Czeiter E, Amrein K, Koller A, 2016. Traumatic brain injury-induced autoregulatory dysfunction and spreading depression-related neurovascular uncoupling: Pathomechanisms, perspectives, and therapeutic implications. Am. J. Physiol. Heart Circ. Physiol 311 (5), H1118–H1131. 10.1152/ajpheart.00267.2016. [PubMed: 27614225]

Tsujikawa A, Ogura Y, 2012. Evaluation of leukocyte-endothelial interactions in retinal diseases. Ophthalmologica 227 (2), 68–79. 10.1159/000332080. [PubMed: 21997258]

Vagnozzi R, Tavazzi B, Signoretti S, Amorini AM, Belli A, Cimatti M, Lazzarino G, 2007. Temporal window of metabolic brain vulnerability to concussions: mitochondrial-related impairment–part I. Neurosurgery 61 (2), 379–388 discussion 388–379. 10.1227/01.NEU.0000280002.41696.D8. discussion 388–379.

Vedung F, Fahlstrom M, Wall A, Antoni G, Lubberink M, Johansson J, Marklund N, 2022. Chronic cerebral blood flow alterations in traumatic brain injury and sports-related concussions. Brain Inj. 36 (8), 948–960. 10.1080/02699052.2022.2109746. [PubMed: 35950271]

Wang ML, Li WB, 2016. Cognitive impairment after traumatic brain injury: the role of MRI and possible pathological basis. J. Neurol. Sci 370, 244–250. 10.1016/j.jns.2016.09.049. [PubMed: 27772768]

Ware JB, Dolui S, Duda J, Gaggi N, Choi R, Detre J, Kim JJ, 2020. Relationship of cerebral blood flow to cognitive function and recovery in early chronic traumatic brain injury. J. Neurotrauma 37 (20), 2180–2187. 10.1089/neu.2020.7031. [PubMed: 32349614]

Wilson L, Stewart W, Dams-O'Connor K, Diaz-Arrastia R, Horton L, Menon DK, Polinder S, 2017. The chronic and evolving neurological consequences of traumatic brain injury. Lancet Neurol. 16 (10), 813–825. 10.1016/S1474-4422(17)30279-X. [PubMed: 28920887]

Xu L, Ware JB, Kim JJ, Shahim P, Silverman E, Magdamo B, Sandsmark DK, 2021. Arterial spin labeling reveals elevated cerebral blood flow with distinct clusters of hypo- and Hyperperfusion after traumatic brain injury. J. Neurotrauma 38 (18), 2538–2548. 10.1089/neu.2020.7553. [PubMed: 34115539]

Xu C, Li Q, Gao Y, Huo H, Zhang W, 2022. Changes and influencing factors of stress disorder in patients with mild traumatic brain injury stress disorder. Biomed. Res. Int 2022, 9082946. 10.1155/2022/9082946.

Zhang W, Li S, Li K, Li LI, Yin P, Tong G, 2021. The role of protein arginine methyltransferase 7 in human developmentally arrested embryos cultured in vitro. Acta Biochim. Biophys. Sin. Shanghai 53 (7), 925–932. 10.1093/abbs/gmab068. [PubMed: 34041522]

Zhang S, Wu X, Wang J, Shi Y, Hu Q, Cui W, Qu Y, 2022. Adiponectin/AdiopR1 signaling prevents mitochondrial dysfunction and oxidative injury after traumatic brain injury in a SIRT3 dependent manner. Redox Biol. 54, 102390 10.1016/j.redox.2022.102390.

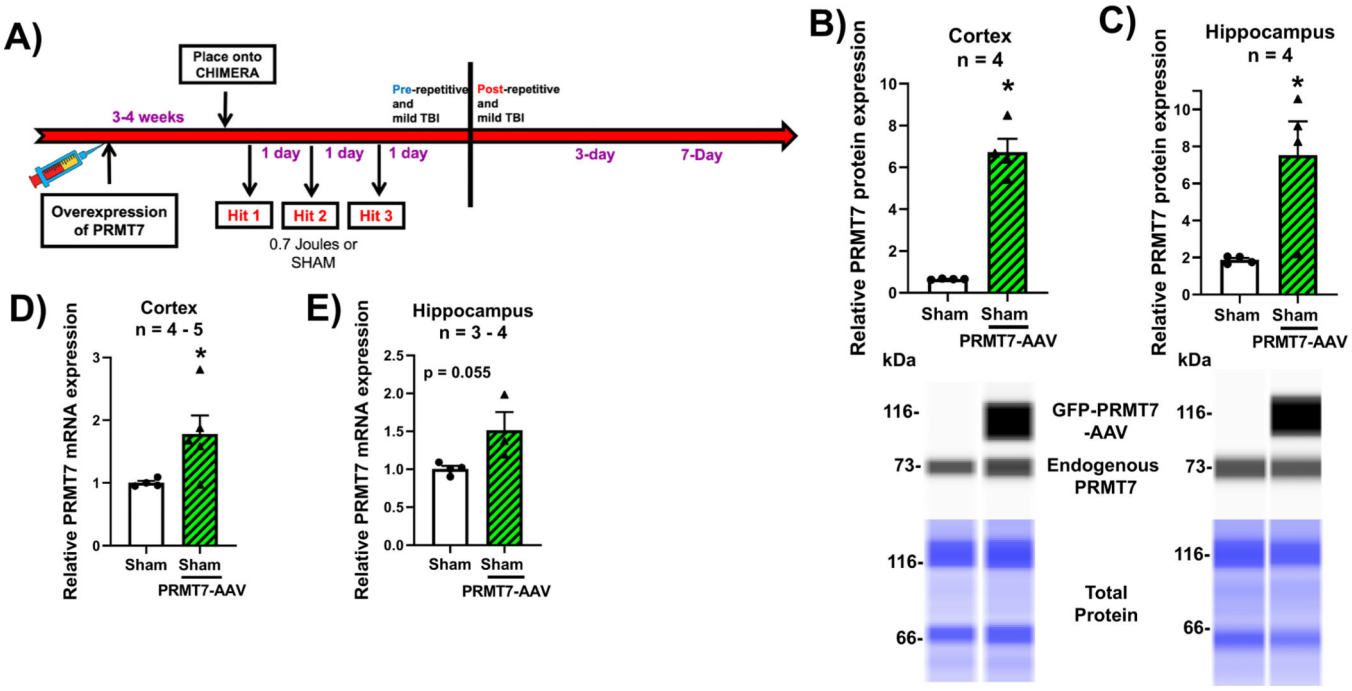

Fig. 1.

rmTBI mice overexpressed with PRMT7-AAV enhanced protein levels. A) Cartoon illustrating the experimental design of PRMT7-AAV overexpression virus (AAV/PHP.eB-hSYN1-GFP.mPRMT7-WPRE) in rmTBI. Mice were injected intravenously 3–4 weeks prior to experimentation, exposed to three repetitive and mild TBI hits, separated by 24 h intervals and assessed at 3 and 7 days post-rmTBI. PRMT7 protein expression (~73 kDa) was significantly elevated in the B) cortex (green bar/black lines) and the C) hippocampus (green bar/black lines) relative to SHAM mice (white bars), measured by capillary-based immunoassay and normalized to total protein. Computer software generated pseudo-blots are presented below each of the corresponding protein graphs where applicable. PRMT7 mRNA expression was also assessed and revealed significant upregulation in the D) cortex and a trending increase in the E) hippocampus (green bar/black lines) relative to SHAM (white bars). Results were expressed as mean ± SEM. $*p \leq 0.05$, as compared to age-matched rmTBI mice, evaluated by Student's *t*-test. ($n = 3–5$).

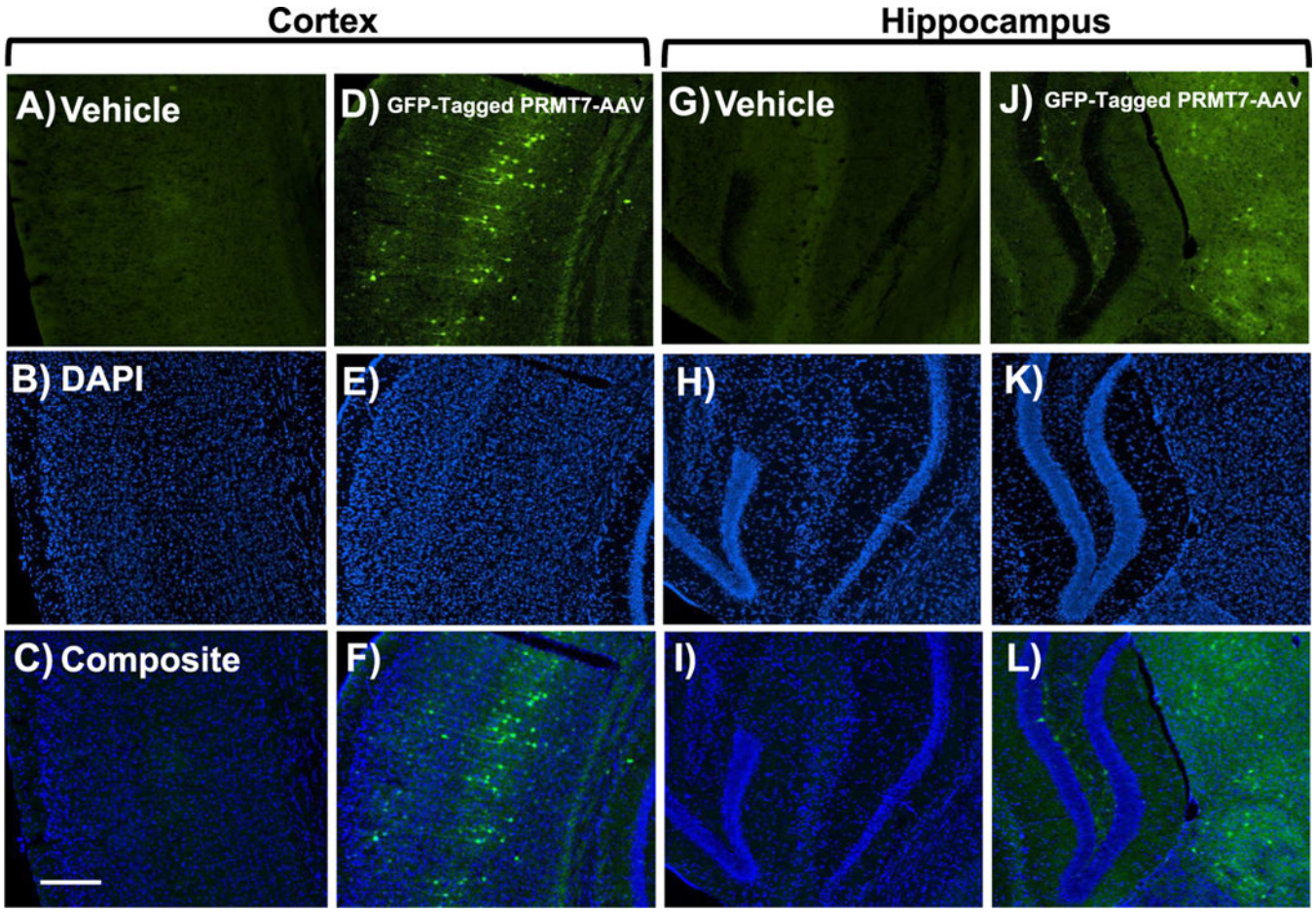

Fig. 2.

rmTBI mice were overexpressed with GFP-tagged PRMT7-AAV. PRMT7-AAV overexpression virus (AAV/PHP.eB-hSYN1-GFP.mPRMT7-WPRE) was injected intravenously and analyzed via histology. Vehicle-treated mice were injected with equal volume of Lactated Ringer's and visualized with confocal microscopy. Vehicle-treated mice did not exhibit GFP-tagged PRMT7-AAV overexpression in histological sections in the cortex A) vehicle B) DAPI stained for nuclei C) composite image. In PRMT7-AAV overexpressed mice, there was robust GFP-tagged PRMT7-AAV expression within the neurons of the D) cortex, E) DAPI for nuclei, F) composite image. The hippocampus revealed the same trend with no GFP expression in the G) vehicle-treated mice, H) DAPI, I) composite, as compared to the J) GFP-PRMT7 AAV treated mice, K) DAPI, L) composite image. Scale bar = 100 μm.

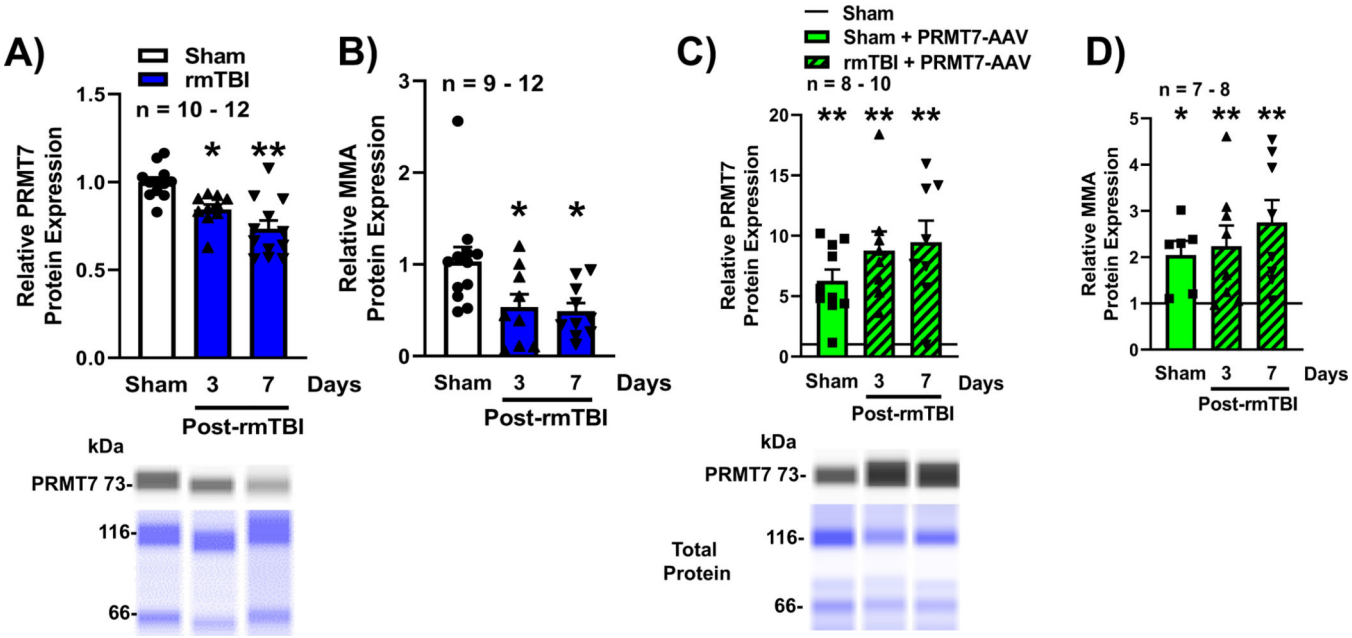

Fig. 3.

Brain PRMT7 protein levels and activity (via MMA) were decreased after rmTBI in C57BL/6 J mice, but enhanced with PRMT7-AAV. A) Protein expression of PRMT7 was reduced 3 and 7 days post-rmTBI (blue bars) relative to SHAM (white bar). B) Reduced expression of PRMT7 in rmTBI mice also had reduced levels of mono-methylarginine (MMA = PRMT7 enzymatic end-product) (blue bars) as compared to SHAM (white bar). C) Overexpression of PRMT7 via PRMT7-AAV was confirmed in all AAV groups (green bar/black lines) and was significantly higher as compared to SHAM mice (black line) without PRMT7-AAV. D) Overexpression of PRMT7-AAV resulted in higher PRMT7 activity, as higher MMA (MMA = PRMT7 enzymatic end-product) was present in all AAV groups (green bar/black lines) v. no AAV SHAM group (black line). In Figs. 3 C & D, all data were calculated based on SHAM group represented by a solid black line. Proteins were measured by capillary-based immunoassay and normalized to total protein. Computer software generated pseudo-blots are presented below each of the corresponding protein graphs where applicable. *$p \leq 0.05$, **$p \leq 0.001$ vs. SHAM, via one-way ANOVA followed by Tukey's *post-hoc* analysis. (For interpretation of the references to colour in this figure legend, the reader is referred to the web version of this article.)

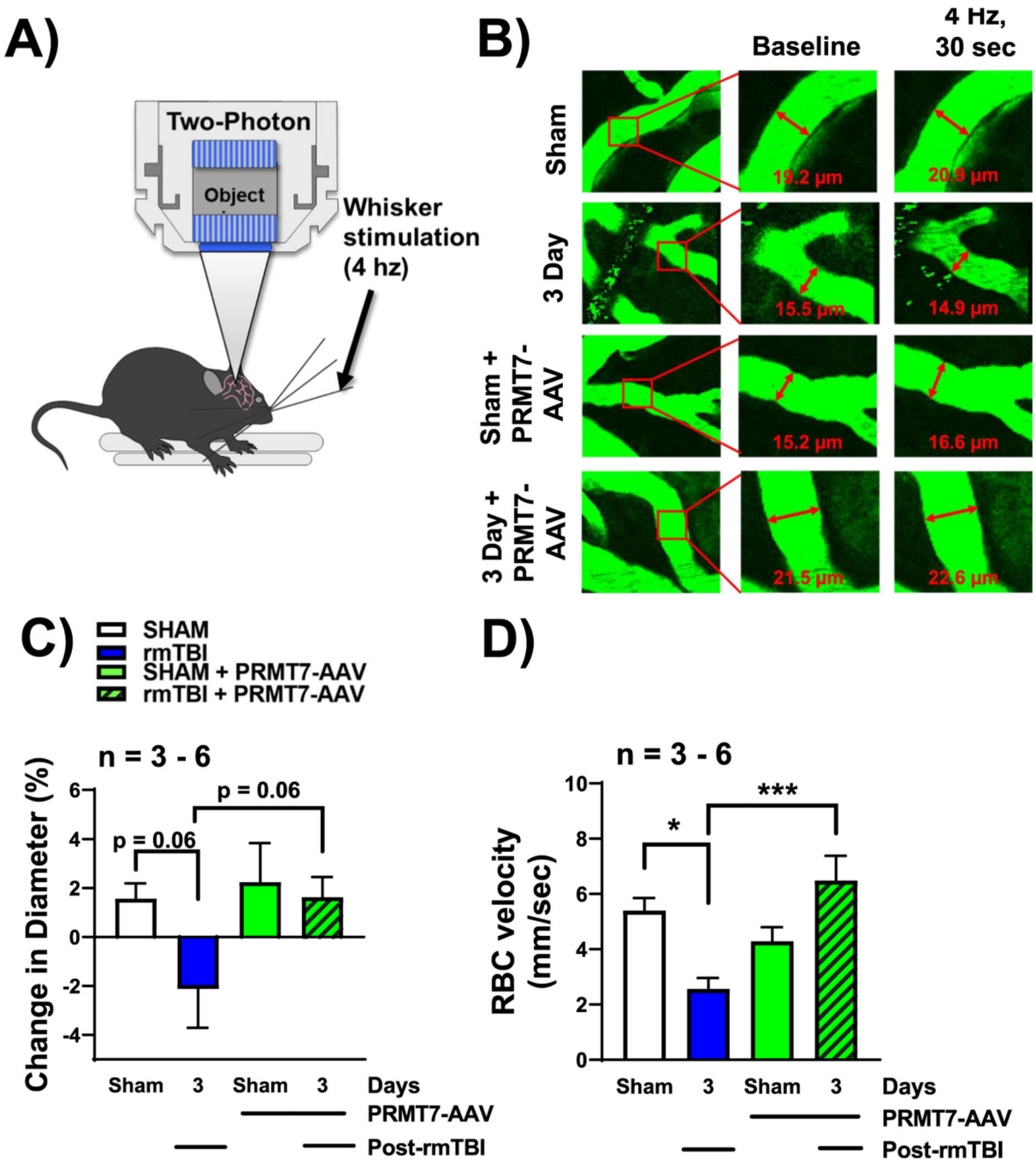

Fig. 4.

Overexpression of PRMT7-AAV prevented neurovascular uncoupling 3 days post-rmTBI in C57BL/6J mice. A) Neurovascular coupling was evaluated based on vascular tonicity changes in response to whisker stimulation (30 s, 4 Hz) concurrent with two-photon laser scanning microscopy. B) Representative images of cortical microvessel visualization via intravenous FITC-dextran injection (Z = 100 µm depth). The thin-skulled procedure produced a circular cranial window ~2 mm from the bregma and 2 mm from the centerline of the skull. C) Microvessel diameters were measured before/after whisker stimulation

in SHAM mice (white bars), 3 days post-rmTBI in mice without (blue bars), SHAM + PRMT7-AAV mice (green bar), and in 3 days post-rmTBI mice + PRMT7-AAV (green bars/black lines). The 3 day rmTBI mice (blue bar) had decreased vessel diameter in response to whisker stimulation contrary to their SHAM counterparts (white bar). Microvessel diameters were increased in rmTBI mice (green bar/black lines) with PRMT7-AAV overexpression to suggest recovery of neurovascular uncoupling. In addition, D) Red blood cell (RBC) velocity was significantly decreased 3 days post-rmTBI (blue bar) relative to SHAM (white bar) but reversed to nominal levels in 3 day rmTBI + PRMT7-AAV (green bar/black lines). $*p \leq 0.05$, $***p \leq 0.001$ determined via one-way ANOVA with Tukey's *post-hoc* analysis. (For interpretation of the references to colour in this figure legend, the reader is referred to the web version of this article.)

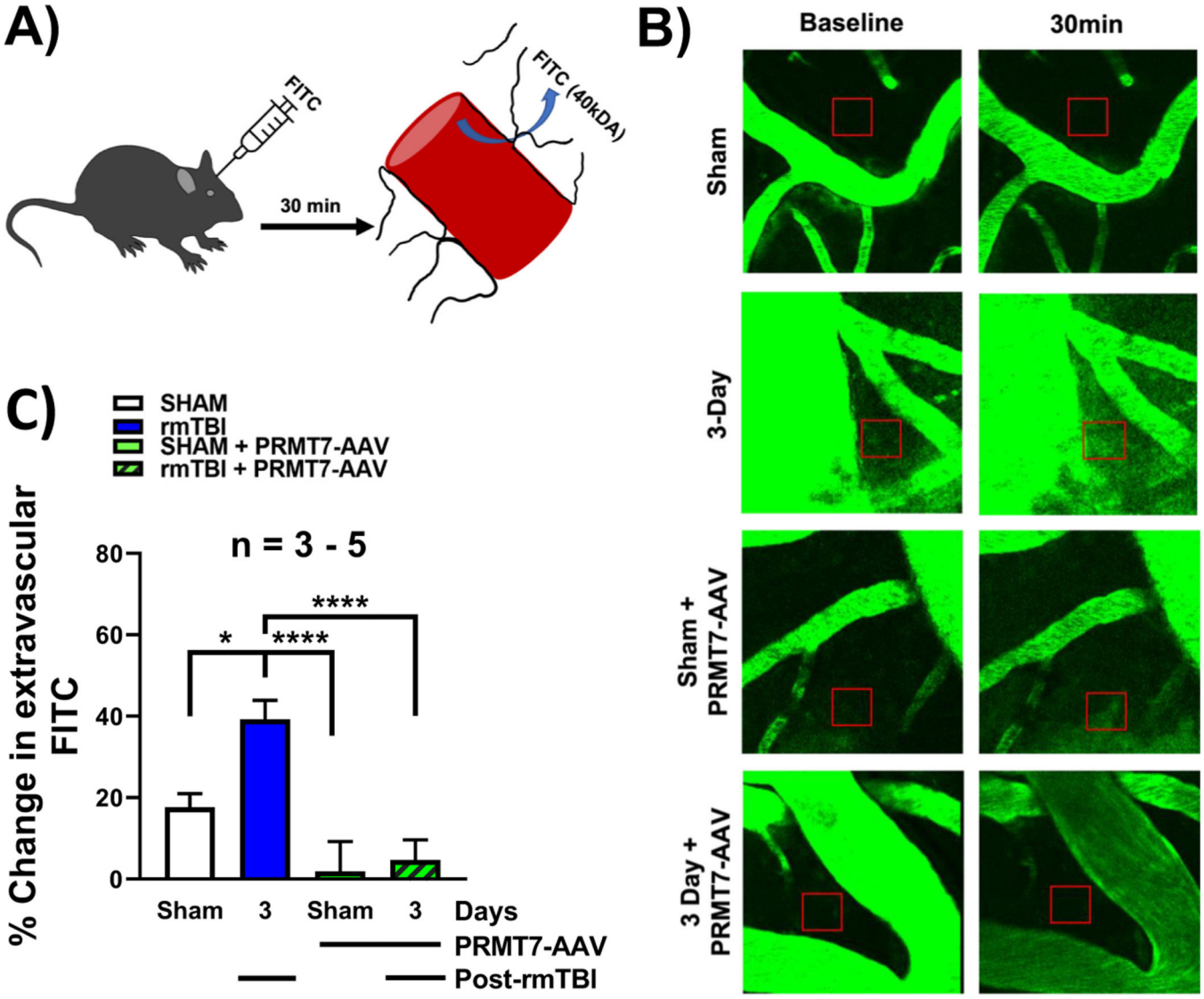

Fig. 5.

Overexpression of PRMT7-AAV prevented blood-brain barrier leakage 3 days post-rmTBI in C57BL/6J mice. A) Schematic representation of the experimental paradigm. B) Representative images of FITC used to visualize brain micro vessels and measure leakage into the perivascular space. C) Higher levels of extravascular low molecular weight (40 kDa) FITC were detected in 3 days post-rmTBI mice (blue bar), relative to sham (white bar) and sham PRMT7-AAV (green bar). PRMT7-AAV overexpression was able to rescue BBB leakage as indicated by the significant reduction in FITC extravasation 3 days post-rmTBI (green bar/black lines) relative to 3 day post-rmTBI mice with no virus. Fluorescence intensity was measured 30 min post-injection within the perivascular region of interest (ROI, red box). At least 3–4 ROIs were analyzed per animal. *$p \leq 0.05$, ****$p \leq 0.0001$, evaluated by one-way ANOVA with Tukey's *post-hoc* analysis. (For interpretation of the references to colour in this figure legend, the reader is referred to the web version of this article.)

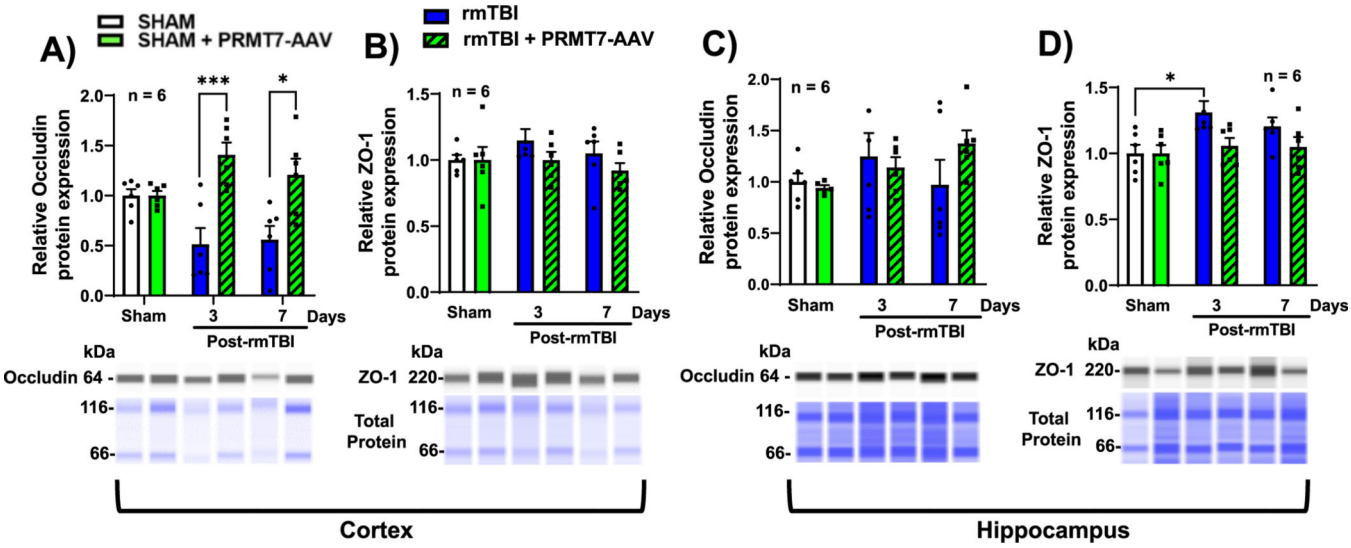

Fig. 6.

Overexpression of PRMT7-AAV enhanced occludin protein levels post-rmTBI in C57BL/6J mice. A) Occludin levels exhibited trending decreases in the cortex at 3 and 7 days post-rmTBI (blue bars) relative to SHAM (white bar). PRMT7-AAV overexpression significantly elevated occludin protein levels (green bar/black lines). B) ZO-1 protein expression was unchanged in the cortex, while no changes in occludin levels were observed in the C) hippocampus. ZO-1 was significantly upregulated in the D) hippocampus at 3 days post-rmTBI with no virus (blue bar) relative to SHAM (white bar). Proteins were measured by capillary-based immunoassay and normalized to total protein. Computer software generated pseudo-blots are presented below each of the corresponding protein graphs when applicable. *$p \leq 0.05$, **$p \leq 0.01$, as evaluated by two-way ANOVA followed Tukey's *post-hoc* analysis. (For interpretation of the references to colour in this figure legend, the reader is referred to the web version of this article.)

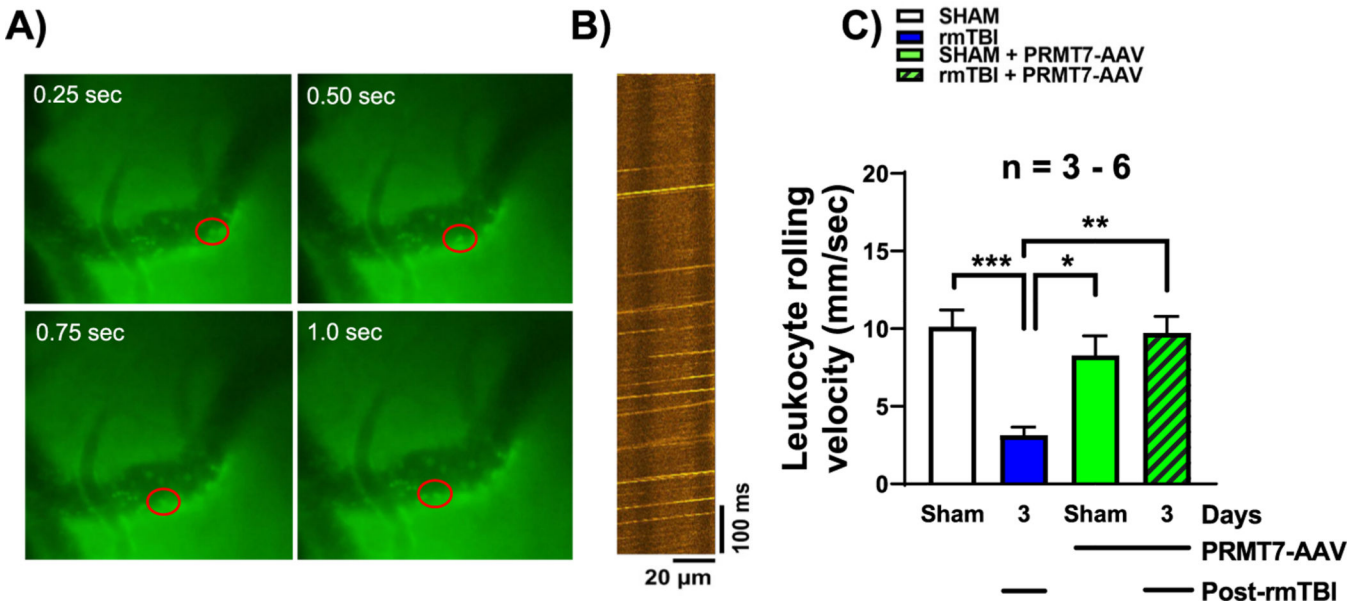

Fig. 7.

Leukocyte rolling velocity was enhanced in mice overexpressing PRMT 7 (via AAV) 3 days post-rmTBI. Two-photon laser scanning microscopy images of rolling leukocytes in microvessels at different time points are shown with A) a red circle with highlighted dot as the leukocyte and B) typical line-scans (512 lines/s) for the measurement of leukocytes labelled with acridine orange. C) 3 days post-rmTBI mice (blue bar) have significantly decreased leukocyte velocities (mm/s) as compared to aged-matched sham mice (white bar). PRMT7-AAV mice (green bar/black lines) had increased velocities at 3 days post-rmTBI v. 3 days post-rmTBI mice with no virus (blue bar). $*p \leq 0.05$, $**p \leq 0.01$, $***p \leq 0.001$. Evaluated by one-way ANOVA with Tukey's *post-hoc* analysis. (For interpretation of the references to colour in this figure legend, the reader is referred to the web version of this article.)

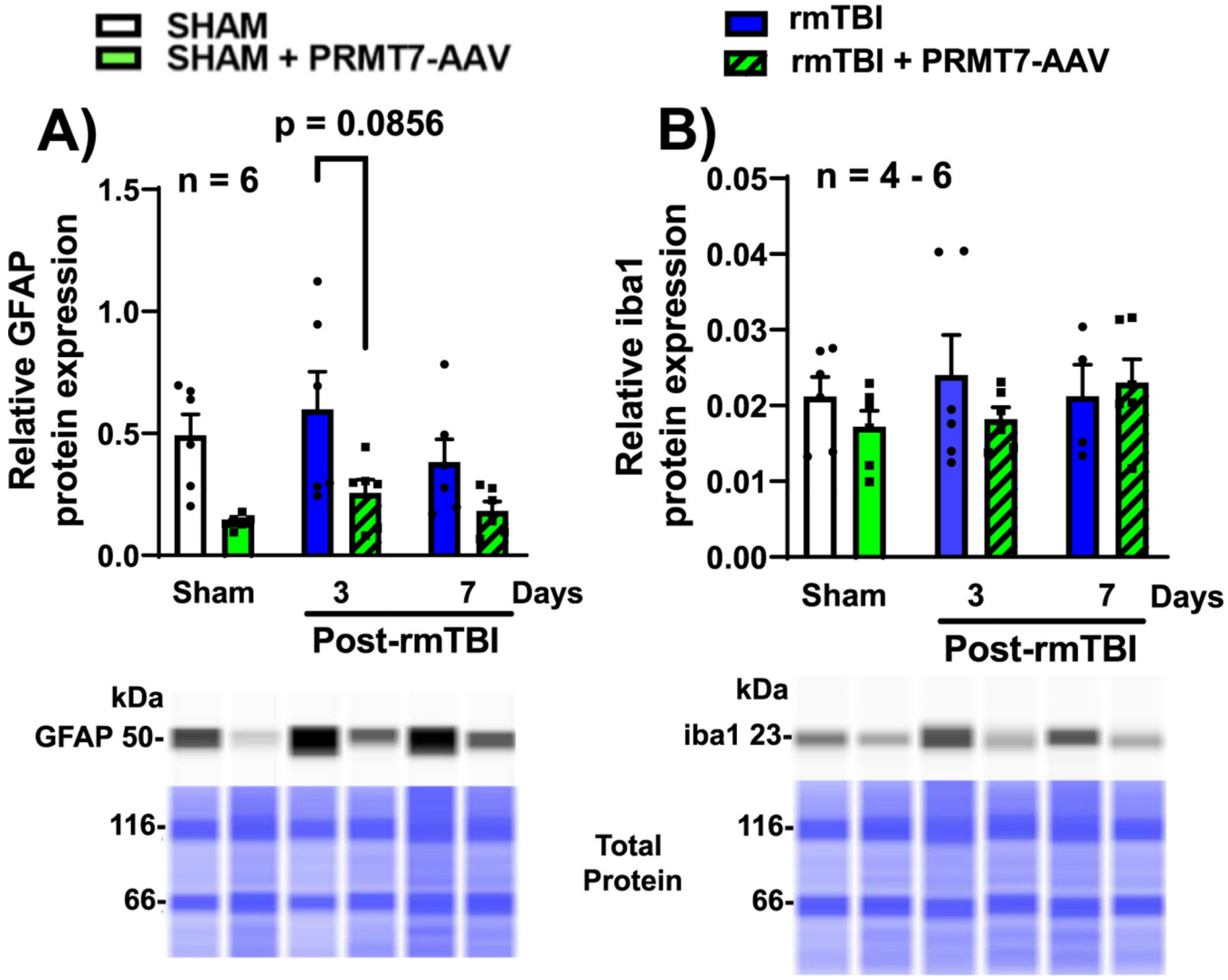

Fig. 8.

Overexpression of PRMT7-AAV improved gliosis in hippocampus. PRMT7-AAV overexpressed mice were assessed for astrogliosis and microgliosis. A) There were trending increases in GFAP protein expression at 3 and 7 days post-rmTBI (blue bars) relative to SHAM (white bar). PRMT7-AAV overexpression revealed strong trending decreases in GFAP expression at 3 and 7 days post-rmTBI (green bar/black lines) relative to 3 and 7 days rmTBI mice with no virus. B) There were trending increases in iba1 levels in 3 and 7 days post-rmTBI mice (blue bars) relative to SHAM (white bar); accompanied by trending decreases in iba1 protein expression in 3 and 7 days + PRMT7-AAV overexpressed rmTBI mice (green bar/black lines) relative to 3 and 7 day rmTBI mice with no virus (blue bars). Proteins were measured by capillary-based immunoassay and normalized to total protein. Computer software generated pseudo-blots are presented below each of the corresponding protein graphs where applicable. *$p \leq 0.05$ evaluated by one-way ANOVA with Tukey's *post-hoc* analysis. (For interpretation of the references to colour in this figure legend, the reader is referred to the web version of this article.)

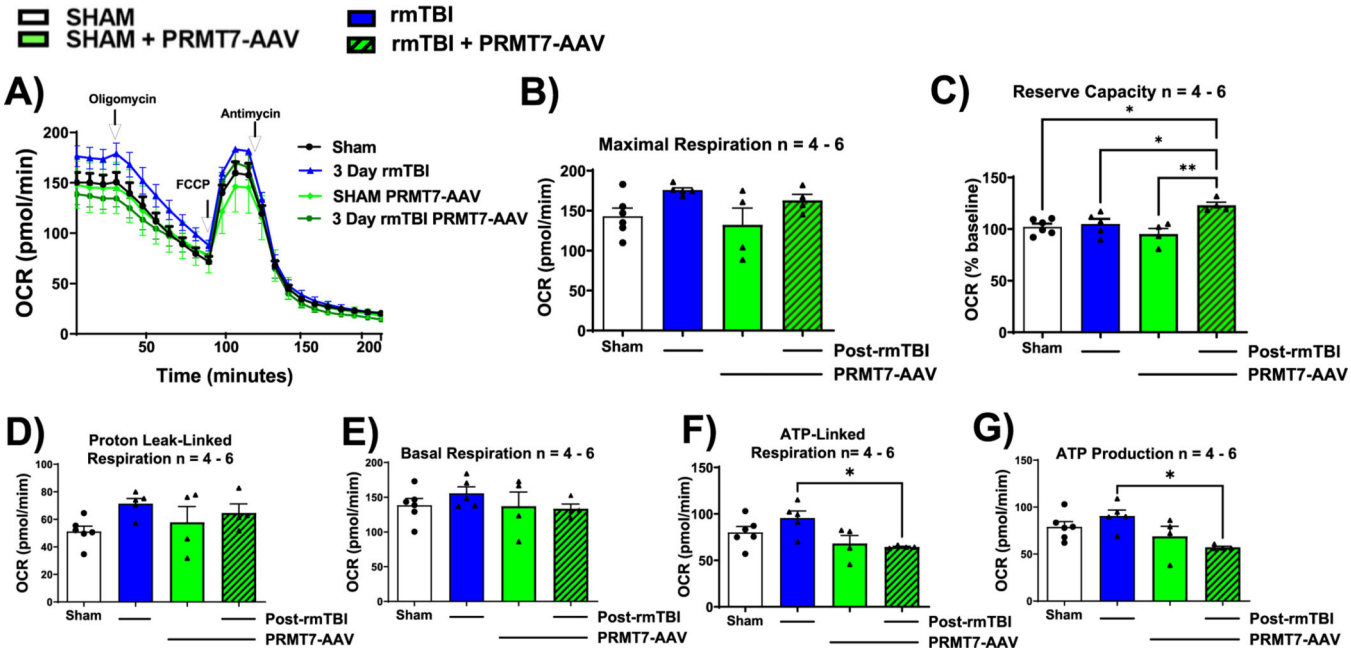

Fig. 9.

PRMT7-AAV enhanced mitochondrial reserve capacity in the CA1 region of the hippocampus. Oxygen consumption rates were measured at 1, 3 and 7 days post-rmTBI and the results suggest 3 days post-rmTBI had the most robust changes, therefore, we intervened at day 3 with PRMT7-AAV. A) Tracing of oxygen consumption rates (OCR) of each time point SHAM (white) 3 day (blue) SHAM + PRMT7-AAV (green) 3 days post-rmTBI + PRMT7-AAV overexpression (green bar/black lines). B) While we observed no significant changes in maximal respiration, C) reserve capacity was significantly enhanced with overexpression of PRMT7-AAV + 3 days post-rmTBI (green bar/black lines) relative to SHAM (white bar), 3 days post-rmTBI (blue bar), and SHAM + PRMT7-AAV (green bar). In addition, there were no changes in D) proton-leak-linked respiration or E) basal respiration. F) ATP-linked respiration was reduced at 3 days post-rmTBI + PRMT7-AAV (green bar/black lines) relative to 3 days post-rmTBI mice + no virus (blue bar). G) ATP production was significantly decreased at 3 days post-rmTBI + PRMT7-AAV (green bar/black lines) relative to 3 day rmTBI mice + no virus (blue bar). Results were expressed as mean ± SEM. *$p \leq 0.05$, evaluated by one-way ANOVA with Tukey's *post-hoc* test ($n = 4–6$). (For interpretation of the references to colour in this figure legend, the reader is referred to the web version of this article.)

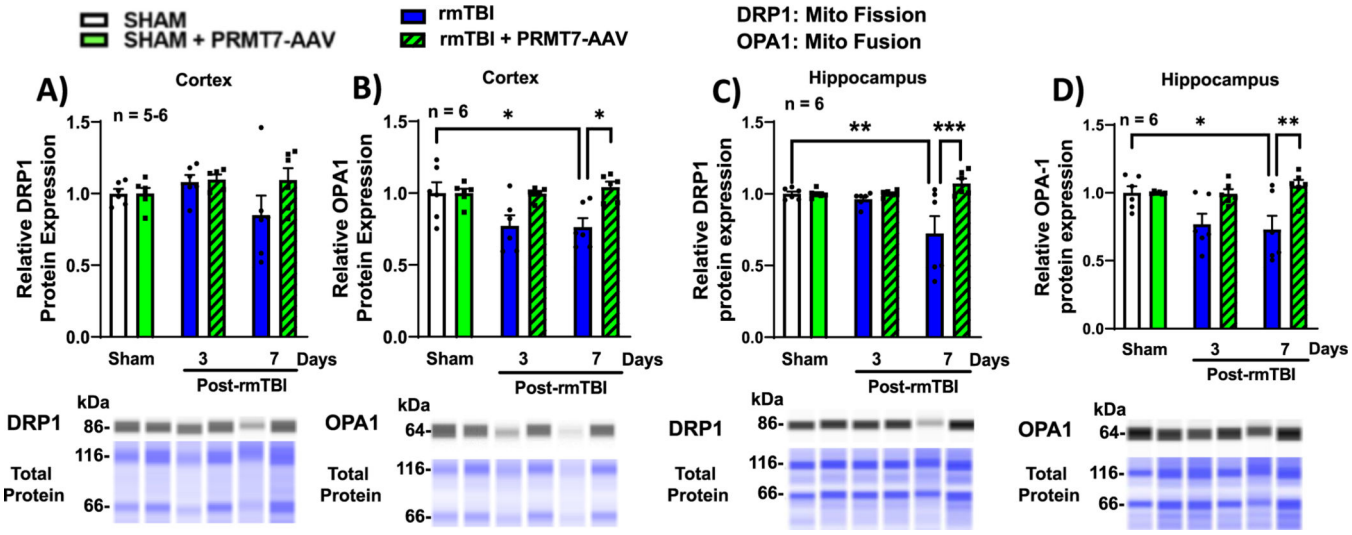

Fig. 10.

PRMT7-AAV normalized mitochondrial fission and fusion dynamics after rmTBI in C57BL/6 J mice. Fission (DRP1) and fusion (OPA1) mitochondrial markers were assessed in the cortex and hippocampus. A) DRP1 protein levels were unchanged in the cortex, while B) OPA1 protein levels were decreased in the cortex at 7 days post rmTBI (blue bar) relative to SHAM (no virus – white bar), whereas PRMT7-AAV (green bar/black lines) increased OPA1 to nominal levels as compared to 7 days post-rmTBI mice + no virus (blue bars). C) DRP1 levels were lower in the hippocampus at 7 days post rmTBI (blue bar) relative to SHAM (white bar) and PRMT7-AAV enhanced DRP1 levels at 7 days post-rmTBI (green bar/black lines) relative 7 days post-rmTBI + no virus (blue bar). Lastly, D) OPA1 levels were reduced in 7 days rmTBI mice (blue bar) relative to SHAM (white bar) and enhanced to control levels with the administration of PRMT7-AAV (green bar/black lines). Proteins were measured by capillary-based immunoassay and normalized to total protein. Computer software generated pseudo-blots are presented below each of the corresponding protein graphs when applicable. *$p \leq 0.05$, **$p \leq 0.01$, ***$p \leq 0.001$; as evaluated by two-way ANOVA followed by Tukey's *post-hoc* analysis.